Geochemistry Geophysics Geosystems G3

Article
Volume 14, Number 7
15 July 2013
doi: 10.1002/ggge.20138
ISSN: 1525-2027

Published by AGU and the Geochemical Society

Multistage collapse of eight western Canary Island landslides in the last 1.5 Ma: Sedimentological and geochemical evidence from subunits in submarine flow deposits

J. E. Hunt, R. B. Wynn, P. J. Talling, and D. G. Masson
National Oceanography Centre, University of Southampton, Southampton, UK (jeh2g08@soton.ac.uk)

[1] Volcaniclastic turbidites in the Madeira Abyssal Plain provide a record of major landslides from the Western Canary Islands in the last 1.5 Ma. These volcaniclastic turbidites are composed of multiple fining-upward turbidite sands, known as subunits. The subunits indicate that the landslides responsible for the sediment gravity flows occurred in multiple stages. The subunits cannot result from flow reflection or splitting because the compositions of volcanic glasses from each individual subunit in an event bed are subtly different. This indicates that each subunit represents a discrete failure as part of a multistage landslide. This has significant implications for geohazard assessments, as multistage failures reduce the magnitude of the associated tsunami. The multistage failure mechanism reduces individual landslide volumes from up to 350 km^3 to less than 100 km^3. Thus although multistage failure ultimately reduce the potential landslide and tsunami threat, the landslide events may still generate significant tsunamis close to source.

Components: 14,391 words, 11 figures, 3 tables.

Keywords: Canary Islands; submarine landslide; turbidites; subunits; multistage collapse.

Index Terms: 3000 Marine Geology and Geophysics: Submarine landslides; 1800 Hydrology: Sediment transport; 4500 Oceanography: Physical; Sediment transport; 8400 Volcanology: Volcanic hazards and risks; 4300 Natural Hazards: Geological; Risk; Disaster risk analysis and assessment.

Received 16 November 2012; **Revised** 8 March 2013; **Accepted** 10 March 2013; **Published** 15 July 2013.

Hunt, J. E., R. B. Wynn, P. J. Talling, and D. G. Masson (2013), Multistage collapse of eight western Canary Island landslides in the last 1.5 Ma: Sedimentological and geochemical evidence from subunits in submarine flow deposits, *Geochem. Geophys. Geosyst.*, *14*, 2159–2181, doi:10.1002/ggge.20138.

1. Introduction

[2] The evolution of oceanic volcanic islands is typified by periods of rapid volcanic construction punctuated by large-scale flank collapses. Volcanic island landslides can involve volumes greater than 100 km^3 and are amongst the largest mass movements in the world [*Siebert*, 1982; *Moore et al*., 1989, 1994; *Masson et al*., 2002; *Hunt et al*., 2013]. Large-volume landslides have been reported from the Canary Islands [*Holcomb and Searle*, 1991; *Watts and Masson*, 1995, 2001; *Masson et al*., 2002], Cape Verde archipelago [*Le Bas et al*., 2007; *Masson et al*., 2008], Réunion Island [*Lenát et al*., 1989; *Labazuy*, 1996; *Oehler et al*., 2004, 2008], and Hawaiian archipelago [*Moore et al*., 1989, 1994; *McMurtry et al*., 2004). In the last 2 million years alone there have been 11 landslides in the

Canary Islands [*Masson et al*., 2002; *Acosta et al*., 2003]. Eight of these events have been large enough to generate voluminous turbidites in the neighboring Madeira Abyssal Plain [*Hunt et al*., 2013].

[3] Due to the potential geohazards associated with future volcanic island flank collapses, it is important to understand how they are emplaced. The style of failure and emplacement on the sea floor can have implications for tsunamigenesis. Whether the failure is multistage or single block, retrogressive or progressive, submarine or subaerial, and disintegrative or not, can affect tsunamigenesis [*Harbitz et al*., 1992, 1993, 2006; *Fine et al*., 2001, 2003; *Ward*, 2001; *Trifunac and Todorovska*, 2002; *Murty*, 2003; *Haugen et al*., 2005; *Løvholt et al*., 2005, 2008; *Giachetti et al*., 2011; *Watt et al*., 2012]. Although the probability of a large-volume Canary Island flank collapse occurring is potentially low, this does not necessarily mean that the risk is low. Risk is dependent both on probability of occurrence and the resultant consequences of such events, namely generation of a tsunami(s) [*Abadi et al*., 2012]. Therefore, determining landslide characteristics of past events will ultimately better inform tsunami modeling and risk assessments.

[4] A future flank collapse has been predicted from the Cumbre Vieja volcano of La Palma, in the Canary Islands [*Ward and Day*, 2001]. This Cumbre Vieja collapse has been modeled as a single block with a volume of 500 km^3 and a thickness of 1400 m [*Ward and Day*, 2001; *Mader*, 2001; *Gisler et al*., 2006]. The resulting tsunami from such an event could inundate the Atlantic coastline of the United States of America and Western Europe [*Ward and Day*, 2001]. More recent modeling suggests that the amplitude of the tsunami wave before run up is 2–5 m [*Gisler et al*., 2006; *Løvholt et al*., 2008]. This is substantially lower than that originally forecast by *Ward and Day* [2001]. However, such a tsunami could still be very destructive, especially in near-field areas of the Canary Islands and Northwest Africa [*Abadi et al*., 2012].

[5] Modeling of the Cumbre Vieja collapse from La Palma [*Ward and Day*, 2001; *Mader*, 2001; *Gisler et al*., 2006], 1888 Ritter Island landslide [*Ward and Day*, 2003], and 1988 landslide from Stromboli [*Tinti et al*., 1999, 2000] have utilized single sliding-block models. However, there is growing evidence to suggest that volcanic island flank collapses are not necessarily single-block failures, but may occur as multistage and potentially retrogressive failures [*Garcia and Hull*, 1994; *Garcia*, 1996; *Wynn and Masson*, 2003; *Di Roberto et al*., 2010; *Giachetti et al*., 2011; *Hunt et al*., 2011]. Whether or not the landslide occurs as a single or multistage failure controls the volume involved in tsunamigenesis at any one given time. The volume of the failure entering the ocean has a first order control on the tsunami wave amplitude [*Murty*, 2003].

[6] Proximal debris avalanche terrains are complex areas suffering from erosion and overprinting of events [*Watts and Masson*, 1995, 2001; *Urgeles et al*., 2001; *Masson et al*., 2002]. As a consequence, studies have begun to focus on the characteristics of sediment gravity flows generated by landslides [*Garcia and Hull*, 1994; *Garcia*, 1996; *Wynn and Masson*, 2003; *Di Roberto et al*., 2010; *Hunt et al*., 2011]. In addition to determining the source, timing and magnitude of landslides, turbidites can provide information on the failure mechanism [*Wynn and Masson*, 2003; *Di Roberto et al*., 2010; *Hunt et al*., 2011]. A stacked sequence of interbedded turbidite sands and mud (subunits) within a single event bed has been interpreted to demonstrate an originally multistage landslide [*Hunt et al*., 2011, and references therein]. However, to test whether occurrence of multistage volcanic island landslides is common, it is important to examine further events in detail.

[7] Agadir Basin represents a depocentre proximal to the Canary Islands that is not fed by complex channel systems (Figure 1). *Wynn and Masson* [2003] inferred that the subunits present in the El Golfo and Icod beds within this basin represent multistage failures. *Hunt et al*. [2011] investigated the Icod deposit in the Agadir Basin, but focussed on volcanic glass analyses on a proximal location to the island (site JC27/02). The first objective of the present study is to analyze volcanic glass compositions from subunit intervals in these two beds within Agadir Basin. This initial aim determines whether subunits in the El Golfo and Icod deposits in Agadir Basin represent multistage failures, as originally posed by *Wynn and Masson* [2003]. Consistency between compositions of different Icod subunits from proximal and basinal sites would also show that subunits can be geochemically correlated over distances >300 km from source.

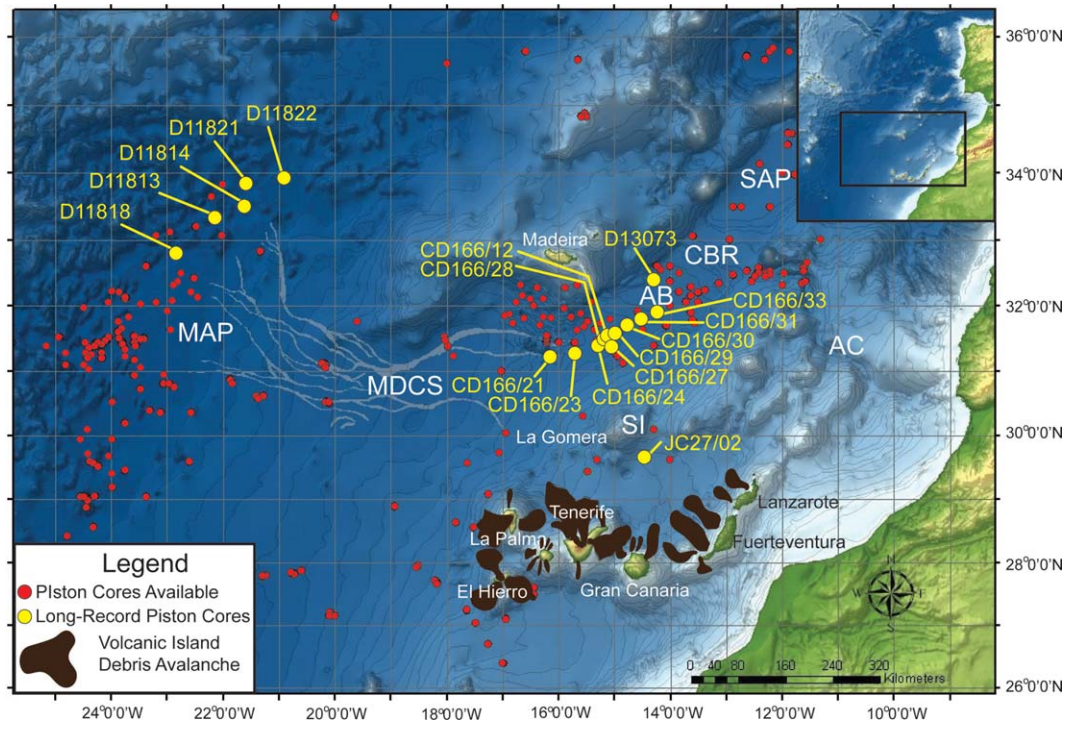

Figure 1. Map of the Moroccan Turbidite System offshore Northwest Africa, showing the distribution of Late Quaternary landslides in the Western Canary Islands and cores used in the present investigation to study the sediment gravity flows generated from them. Map based on GEBCO bathymetry. MAP = Madeira Abyssal Plain, MDCS = Madeira Distributary Channel System, AB = Agadir Basin, SI = Selvage Islands, AC = Agadir Canyon, CBR = Casablanca Ridge and SAP = Seine Abyssal Plasin.

[8] In the last 1.5 Ma eight landslides from the Western Canary Islands with volumes >100 km^3 have generated turbidites that reached the Madeira Abyssal Plain (Figure 1), including the El Golfo and Icod landslides [*Hunt et al*., 2013]. The second aim of this paper is to investigate the failure mechanism of all of these Late Quaternary Canary Island landslides. This is achieved by examining the volcaniclastic turbidite record from the Madeira Abyssal Plain. Sedimentological, geochemical and petrophysical studies of the deposits are used to characterize the subunit facies of these beds. Volcanic glass geochemistry from the subunits can determine whether or not these landslides are the product of multistage collapse. Glass compositions of the subunits will also help to test whether the subunits result from flow reflections or from flows splitting and exiting the Madeira channels. Identifying whether or not the majority of recent major landslides from the Canary Islands are multistage is important, since this could show that multistage collapse is a common failure mechanism, and not restricted to isolated case studies.

[9] Landslide activity has also been identified in the Cape Verde and Azores archipelagos, which also lie on slow-moving Atlantic oceanic crust [*Holcomb and Searle*, 1991; *Malbeiro*, 2006; *Le Bas et al*., 2007; *Masson et al*., 2008]. If multistage failure is a more common process in the Canary Islands, this could be the case for submarine landslides from these islands and those from fast-moving geodynamic settings. Indeed, evidence already suggests that multistage submarine landslides occur in the Hawaiian archipelago [*Garcia*, 1996].

2. Geological and Geomorphic Setting

[10] The Canary Islands form an archipelago associated with movement of Jurassic-age (156–176 Ma) Atlantic oceanic crust over a mantle plume [*Klitgort and Schouten*, 1986; *Hoernle and Schmincke* 1993; *Hoernle et al*., 1995; *Carracedo et al*., 1998; *Schmincke et al*., 1998]. The result is a general east-to-west age progression in the islands [*Carracedo*, 1994, 1999; *Carracedo et al*., 1998]. The Western Canary islands of Tenerife, La Palma and El Hierro are the focus of this study, since geologically recent landslide activity has

been recorded onshore and in the proximal submarine aprons [*Masson et al*., 2002, and references therein; *Acosta et al*., 2003, and references therein].

[11] The study area comprises Agadir Basin and the Madeira Abyssal Plain of the Moroccan Turbidite System, on the Northwest African passive margin [*Wynn et al*., 2000, 2002]. Agadir Basin represents a more proximal depocentre to both the Moroccan continental shelf and Canary Islands (Figure 1). Agadir Basin is located in 4200–4400 m water depths and is bound to the north by the Madeira archipelago and south by the Selvagen Islands [*Wynn et al*., 2000, 2002; *Frenz et al*., 2009]. The Madeira Abyssal Plain represents the most distal and deepest depocentre in the Moroccan Turbidite System in 5000–5500 m water depths (Figure 1) [*Weaver and Kuijpers*, 1983; *Weaver et al*., 1992]. The Madeira Abyssal Plain is connected to the more proximal Agadir Basin via the Madeira Distributary Channel System [*Masson*, 1994; *Frenz et al*., 2009; *Stevenson et al*., 2013].

3. Late Quaternary Landslide and Turbidite Histories of the Canary Archipelagos

[12] Submarine landslides have been extensively mapped in the Canary Islands with application of low-frequency seismic reflection and side-scan sonar [*Holcomb and Searle*, 1991; *Watts and Masson*, 1995, 2001; *Masson*, 1996; *Urgeles et al*., 1997, 1999, 2001; *Masson et al*., 1997; *Gee et al*., 2001; *Krastel et al*., 2001; *Wynn et al*., 2000, 2002]. In addition, piston coring in the Madeira Abyssal Plain and Agadir Basin has allowed correlation of dated volcaniclastic turbidites with onshore landslide events [*Masson et al*., 2002, 2006; *Hunt et al*., 2011, 2013]. This section summarizes previous work covering the 1.5 Ma-to-recent record of volcanic island landslides in the Western Canary Islands (Table 1).

3.1. Tenerife

[13] The Icod landslide represents the last major flank collapse to affect northern Tenerife. It has been dated at 165 ± 5 ka by linking the turbidite (Agadir Basin bed A14 and Madeira Abyssal Plain bed Mg), submarine debris avalanche deposit and onshore landslide scar (Table 1) [*Weaver and Rothwell*, 1987; *Watts and Masson*, 1995; *Masson et al*., 2002; *Wynn et al*., 2002; *Wynn and Masson* 2003; *Frenz et al*., 2009; *Hunt et al*., 2011]. Evidence from the deposit in Agadir Basin and on the southern slopes of the Selvagen Islands demonstrates that the Icod landslide was multistage and retrogressive [*Hunt et al*., 2011]. This evidence includes the presence of higher quantities of marine carbonate and altered volcanic glasses in the basal subunit failures compared with the upper subunit failures comprising negligible marine carbonate and only unaltered glasses [*Hunt et al*., 2011]. Furthermore, the geochemistry of the subunits of the Icod deposit indicates a progressive failing of the flank from the basaltic submarine flank to the phonolitic stratocone [Hunt *et al*., 2011].

[14] The Orotava landslide, also off the northern flank of Tenerife, has a suggested age of 540–710 ka, based on onshore dating (Table 1) [*Marti et al*., 1994; *Ancochea et al*., 1999; *Cantagrel et al*., 1999; *Marti and Gudmundsson*, 2000]. Bed

Table 1. Summary of 0–1.5 Ma Volcaniclastic Turbidites from the Madeira Abyssal Plain

Event Name	Biostratigraphic Age[a] (ka)	Photo-spectrometry Age[b] (ka)	ODP Age[c] (ka)	Onshore Age[d] (ka)	Turbidite Volume in Madeira Abyssal Plain[e] (km^3)	Proposed Landslide Volume[d] (km^3)	Island Provenance	Landslide Association
Mb	15±5	15±5	?	12–89	135±15	300±	El Hierro	El Golfo
Mg	165±5	165±5	170	150–170	130±25	320±40	Tenerife	Icod
Mn	480±5	490±5	>443 < 780	125–536	50±15	>145	La Palma	Cumbre Nueva
Mo	540±5	530±5	>443 < 780	540–690	135±30	>210	Tenerife	Orotava
Mp	550±5	540±5	>443 < 780	300–500	90±25	235±20	El Hierro	El Julan
Mz	850±10	850±10	830	780–840	85±40	>85	Tenerife	Güímar
Mab	1050±10	106±10	1050	540–1120	115±30	>115	El Hierro	Tiñor
Maf	1150±10	1180±10	1200	600–1300	50±30	>50 < 500	Tenerife	Roques de García

[a]Ages from positions of turbidites to specific biostratigraphic markers from *Hunt et al*. [2013; authors' Figure 5].
[b]Dates of beds based on position of bed within down-core L^* profile correlated to *Lisiecki and Raymo* [2005] $\delta^{18}O$ curve.
[c]Dates from ODP records of beds based on dating of hemipelagite, from *Hunt et al*. [2013; authors' Figure 7].
[d]Details from Masson *et al*. [2002] and *Hunt et al*. [2013].
[e]Turbidite volumes are decompacted volumes calculated from ODP core based on the method of *Weaver* [2003].

Mo on the Madeira Abyssal Plain represents the Orotava event, with an age of 535 ± 10 ka [*Hunt et al*., 2013]. The Güímar landslide from the eastern flank of Tenerife has been dated at 780–840 ka [*Ancochea et al*., 1990; *Cantagrel et al*., 1999; *Krastrel et al*., 2001; *Masson et al*., 2002; *Giachetti et al*., 2011]. This event potentially produced bed Mz, which has been dated at 850 ± 10 ka (Table 1) [*Hunt et al*., 2013]. The Roques de García landslide represents the oldest flank collapse from northern Tenerife recovered in the piston cores. Onshore dating resolves a broad age range of 0.6–1.7 Ma, however it is potentially represented by bed Maf, with an age of ∼1.2 Ma (Table 1) [*Cantagrel et al*., 1999; *Hunt et al*., 2013].

3.2. La Palma

[15] The Cumbre Nueva landslide represents a collapse from the Cumbre Nueva Ridge at 125–536 ka during volcanism associated with the Taburiente volcano (Table 1) [*Urgeles et al*., 1999, 2001]. Correlation to Madeira Abyssal Plain bed Mn confirms a 485 ± 10 ka date (Table 1) [*Hunt et al*., 2013]. The Cumbre Neuva debris avalanche overlies the older Playa de la Veta complex deposit of unknown age [*Masson et al*., 2002].

3.3. El Hierro

[16] The El Golfo landslide represents the youngest volcanic flank collapse in the Canary archipelago [*Weaver et al*., 1992; *Masson*, 1996]. The landslide has been correlated with bed Mb in the Madeira Abyssal Plain and bed AB2 in Agadir Basin, with an age of 15 ka (Table 1) [*Weaver et al*., 1992; *Wynn et al*., 2002; *Wynn and Masson*, 2003; *Frenz et al*., 2009].

[17] The El Julán landslide affected the southwest flank of El Hierro and contributed to the development of the resulting El Julán apron. *Masson* [1996] provides a potential age range of 320–500 ka for the El Julán landslide, but there are no details on the constraint of this (Table 1). This event is dated at 540 ± 10 ka based on correlation to bed Mp on the Madeira Abyssal Plain [*Hunt et al*., 2013].

[18] The El Tiñor volcano represented the first subaerial volcanism on El Hierro between 1.12 and 0.882 Ma [*Guillou et al*., 1996; *Carracedo et al*., 1999]. In mining galleries within the El Golfo embayment, El Golfo lavas (dated at 543 ka) overlie east-dipping El Tiñor lavas (dated at 1.04 Ma) [*Carracedo et al*., 1999]. The landslide responsible for truncation of the El Tiñor lavas potentially correlates to bed Mab, which is dated at ∼1.05 Ma (Table 1) [*Hunt et al*., 2013].

4. Methodology and Data

[19] A core transect through the centre of the Agadir Basin is used to characterize the turbidites from the most recent El Golfo and Icod landslides (Figure 1). A series of five piston cores from the northern Madeira Abyssal Plain show the most extensive temporal record of volcaniclastic turbidites with the highest sand content (Figure 1). Coccolithophore biostratigraphy and down-core physical properties have been used to constrain the turbidite dates and correlate beds between sites >50 km apart [*Weaver et al*., 1992; *Howe and Sblendorio-Levy*, 1998; *Hunt et al*., 2013].

[20] Subunits can be identified visually as a series of multiple fining-upward turbidite sands with interbedded turbidite muds. These are characterized by a sharp planar basal contact and a lithic- and carbonate-rich basal deposit. Although there is often an intervening finer layer below a subsequent subunit, the sands are often amalgamated in proximal locations.

4.1. Visual and Geotechnical Logging

[21] Visual sedimentological logging was used to assess the sediment record and subunits within the turbidites. Down-core magnetic susceptibility data was obtained at a 0.5 cm resolution using a *GeoTek*™ XYZ core scanner, and was used to aid the correlation of turbidites. Magnetic susceptibility importantly supports identification of volcaniclastic turbidites, whereby positive excursions represent magnetic volcanic sands. Down-core *P*-wave velocity data from the Madeira Abyssal Plain cores was collected using an acoustic profiler. High *P*-wave values signify turbidite sands. *P*-wave velocity and gamma-ray density profiles of Agadir Basin cores were collected using a *GeoTek*™ MSCL at 0.5 cm resolution.

4.2. Laser Diffraction Grain-Size Analysis

[22] Vertical grain-size profiles were completed through targeted examples of the deposits. The profiles aided identification of subunits. Sediment samples (1 cm^3) were added to 30 mL RO water with a 0.05% sodium hexametaphosphate dispersant and shaken for 12 hours. The dispersed sediment mixtures were analyzed using the *Malvern Mastersizer 2000* particle size analyzer. Typically

three aliquots were measured to assess precision. Standard reference materials (SRM) of mean average 32 μm and 125 μm were used to monitor accuracy (reported at <1% standard deviation), while repeat samples were used to further monitor precision (reported at <0.5% standard deviation).

4.3. SEM Volcanic Glass Analysis

[23] Bulk geochemical compositions have been shown to be sufficient to discriminate between subunits [*Hunt et al*., 2011]. However, these bulk geochemical compositions can be affected by hydrodynamic sorting during passage of the turbidity current [*Hunt et al*., 2011]. Analysis of populations of unaltered volcanic glasses of similar size (90–125 μm) enable better refinement of the provenance and comparison of compositional variations between subunits of the same bed (Appendices 1 and 2; supporting information).[1]

[24] Samples (~3 cm^3) were taken from the bases of the subunits within type-examples of the El Golfo and Icod deposits in Agadir Basin and then each of the volcaniclastic turbidites within the Madeira Abyssal Plain. These were sieved for the >63 μm fraction and subjected to acetic acid (0.1 M) leaching to remove carbonate. The volcanic grains were then mounted on a semiconductor pad and imaged using a *Hitachi TM1000* SEM. Unaltered volcanic glasses (preferably 30–50 grains) of 90–125 μm size (length and breadth) and >45 μm thickness were analyzed from each subunit, at 15 kV with a dwell time of 120 s. In some cases too few glasses met the aforementioned criteria, principally due to alteration, and as a result only 20–30 glasses were analyzed. Glasses chosen were simple in morphology, discounting crenulated pumice sharps and bubble glasses, this was to ensure flat surfaces for analysis and that the glasses were thick enough. Selecting glasses of a specific grain size and morphology also reduces the effects of hydrodynamic sorting controlling the geochemical compositions of the glass populations sampled.

[25] Calibrated results were evaluated for accuracy and precision using a series of glass standards produced from international standard reference materials (Appendices 1 and 2). Concentrations between 1 wt % and2 wt % have precisions of 4%–6% of the value, 2–10 wt % values have precisions to within 2%–5%, while those values >10 wt % have precisions of 0.5%–4% (Appendix 3; supporting information). Accuracies were generally within 1%–5% of the certified value for the suite of standard reference materials, where accuracies were higher with increasing concentration.

[1]Additional supporting information may be found in the online version of this article.

5. Results

5.1. Visual Identification of Agadir Basin Subunits

[26] Subunits can be identified visually as a series of multiple fining-upward turbidite sands interbedded with turbidite muds. Each subunit is also characterized by a sharp or erosional basal contact and a lithic- and carbonate-rich basal deposit. As with previous studies [e.g., *Hunt et al*., 2011] a regular series of seven subunits were identified within the Icod event bed in Agadir Basin (SBU1–7) (Figure 2). The three lowermost subunits (SBU1–3) are amalgamated more proximal to source in the western Agadir Basin. However, all seven subunits become readily identified as separate units more distally in the eastern Agadir Basin (e.g., site D13072) (Figure 2).

[27] The El Golfo event bed has five subunits (SBU1–5) in the most proximal sites (CD166/21 and CD166/23) in the western Agadir Basin (Figure 2). These subunits both thin and fine distally. The uppermost subunits are progressively lost eastward along the basin, with four regular subunits seen at core sites CD166/24 and CD166/28, and only three through the remainder of the western basin (CD166/12, CD166/29, and CD166/31) (Figure 2). Examples of the deposit both on the basin margins and distally in the eastern Agadir Basin demonstrate a progressive cut out of subunits to two and finally one. The El Golfo subunits are characterized by a sequence of basaltic- and carbonate-rich laminations at the base, with a more carbonate-rich sequence of muddy silts above.

[28] Visual identification of the subunits is supported by the magnetic susceptibility and *P*-wave profiles. The coarse-to-medium sand subunit bases are distinguished by the peaks in *P*-wave profiles, while the lithic-rich bases are distinguished by peaks in magnetic susceptibility (Figures 2 and 3). Combining sedimentological logs and physical properties analyses with grain-size analyses can further support the identification of subunits within these deposits (Figures 2 and 3). Often the coarse base of a subunit is also lithic-

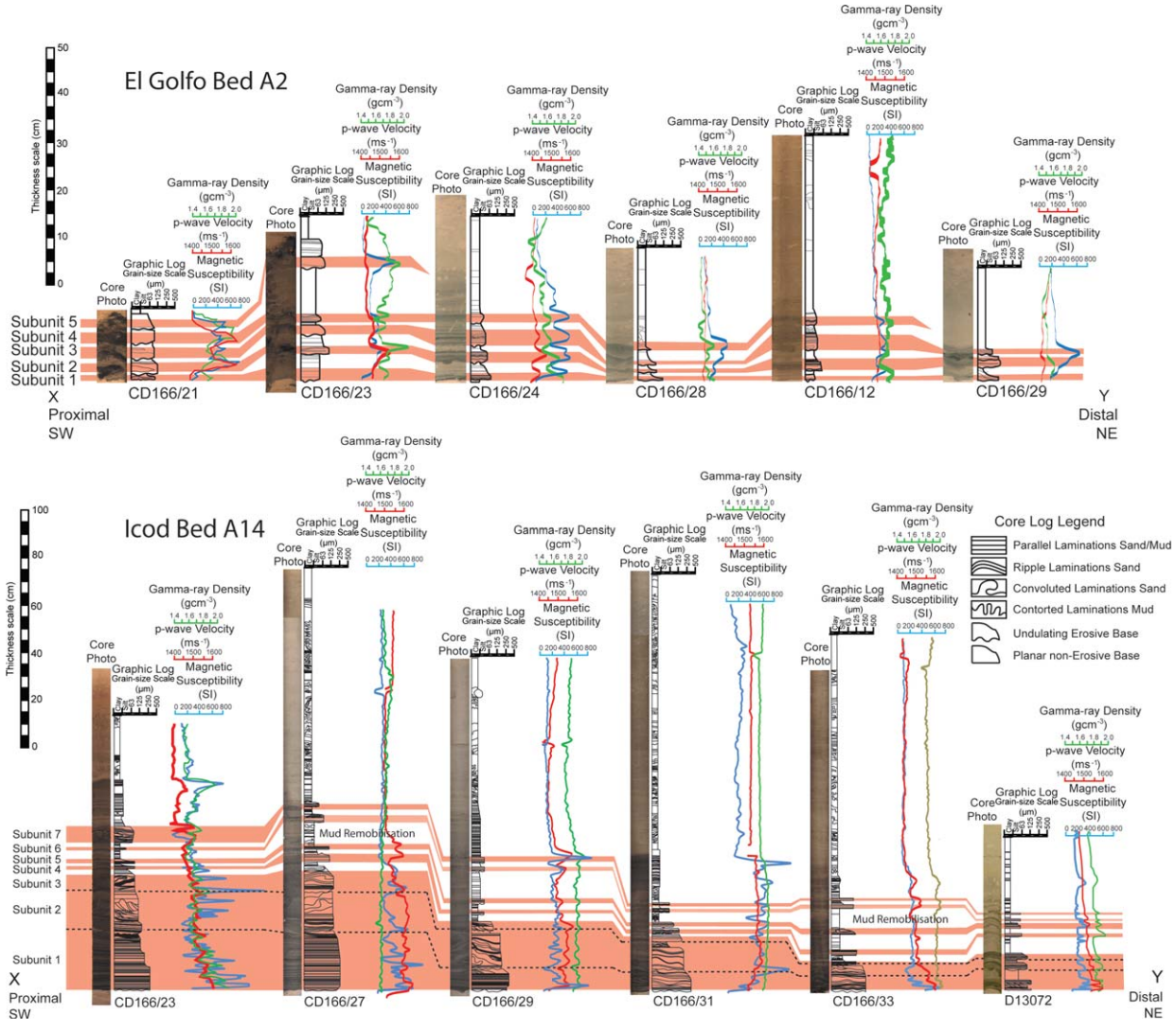

Figure 2. Up-basin correlation panel of the El Golfo and Icod beds in Agadir Basin (core locations on Figure 1). Shows the regular sequence of seven subunits and the ability for these to be highlighted in the petrophysical data (gamma-ray, *P* wave, and magnetic susceptibility).

rich above an erosive basal contact, providing a coincidental excursion in magnetic susceptibility (Figures 2 and 3).

5.2. Grain Specific Geochemistry within Agadir Basin Subunits

[29] This investigation examined volcanic glasses from subunits of the volcaniclastic turbidites. Attention was made to select grains that had not been subjected to alteration, although without SEM backscatter low-level alteration cannot be entirely ruled out. Samples from the subunit intervals of the Icod event bed were taken from site CD166/27. CD166/27 was chosen since it is in the centre of Agadir Basin, and relatively proximal compared to other cores studied.

[30] The total alkali-silica (TAS) diagram delineates compositional fields for the glasses relating to specific igneous rock types (Figure 4b). The glasses fall into the SiO_2 field for Tenerife phonolite and alkali trachyte compositions (Figure 4b). These onshore compositional fields represent data collated from the Max-Plank-Gesellschaft database for geochemistry of rocks of the oceans and continents (GEOROC). Compositional fields for the different Icod subunit glass populations can clearly be delineated (Figure 4b).

[31] For the Icod event bed, the SBU1–2 volcanic glasses from CD166/27 were found to range from basalts to alkali trachyte-trachy andesite in composition. SBU3 had a mixed component composition with alkali trachyte-trachy andesite glasses, but a

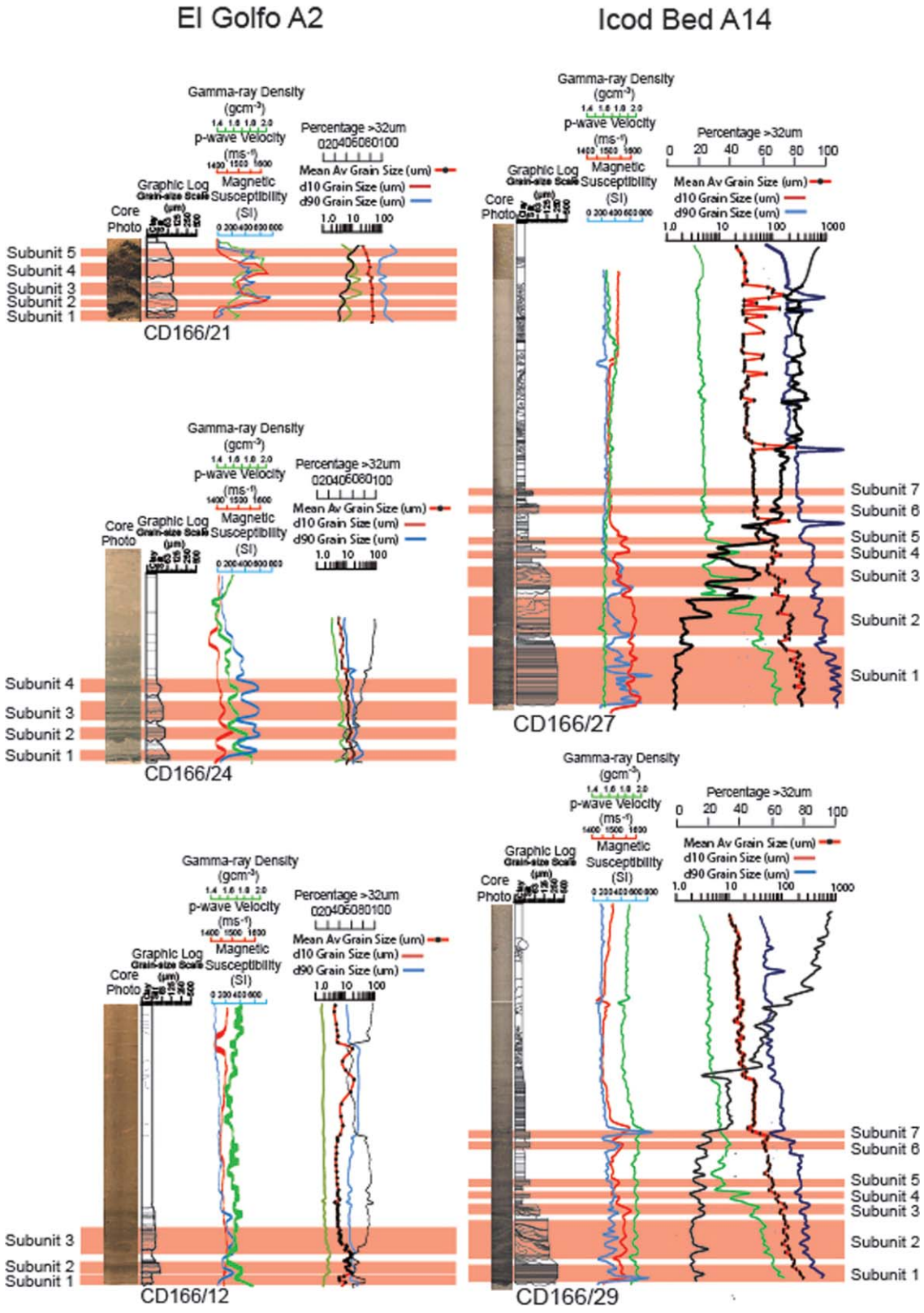

Figure 3. Examples of subunit facies from El Golfo and Icod beds from Agadir Basin. Grain-size data coupled with physical properties.

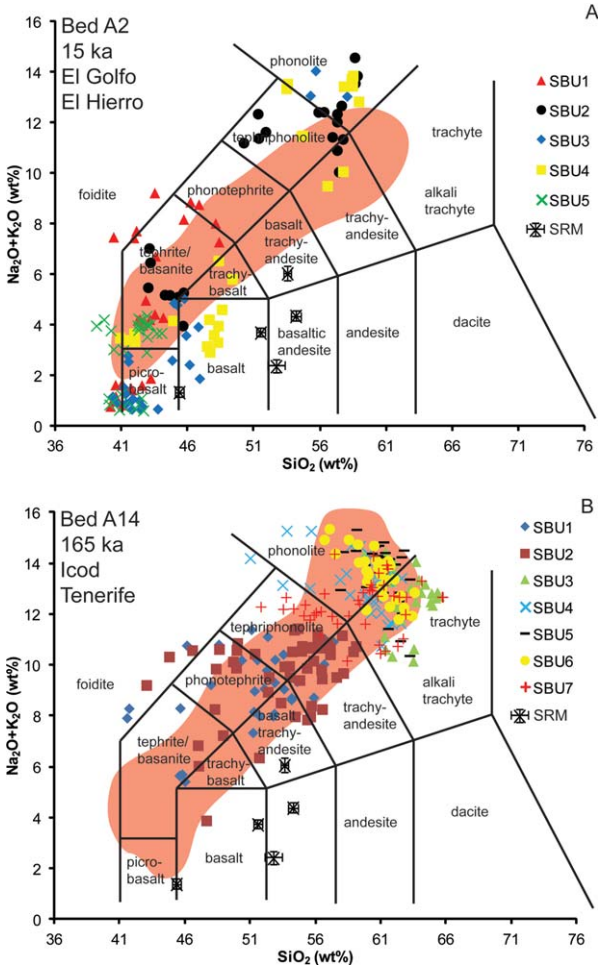

Figure 4. TAS diagrams for the unaltered volcanic glasses taken from the (a) El Golfo landslide bed A2 (site CD166/21) and (b) Icod landslide bed A14 (site CD166/27). SRM analyses indicate the error bars as standard deviation. Red transparency represents the onshore whole-rock compositional range from the GEOROCS database.

predominance of silica-rich alkali-trachyte composition (Figure 4b). SBU4 glasses have a more evolved phonolitic composition, with a proportion of phonolite-trachyte composition. SBU5 and SBU6 glasses lie at the phonolite-alkali trachyte boundary (Figure 4b). Lastly, SBU7 glasses show a different character, composed of strictly tephriphonolite-phonolite glasses (Figure 4b). These results are similar to previous volcanic glass analyses from the subunits of the Icod event bed [*Hunt et al*., 2011]. However, the new additional results show a lower abundance of basaltic glasses in SBU1 and SBU2.

[32] In summary, Icod bed volcanic glasses demonstrate that each subunit forms a disparate compositional field. Within the Icod event bed SBU1 and SBU2 are closely related, with predominantly basic compositions of lower silica and alkali concentrations. SBU3 varies from the trachy-andesite compositions of SBU1 and SBU2 to the evolved compositions of SBU4–6, and also appears to contain glasses with the most evolved compositions. Finally, SBU7 has a different composition to those previous subunits, with relatively low silica but high alkalis (Figure 4b).

[33] The El Golfo volcanic glass compositions are more scattered than the onshore El Hierro whole rock compositional field (Figure 4a). Without the benefit of backscatter, some of the glasses showing greater scatter may reflect low-level alteration. SBU1 for the El Golfo event has a limited composition of volcanic glasses with alkalis <10 wt % and silica <50 wt %. The SBU1 volcanic glasses fall into two compositions of highly basic picrobasalts and basanite-phonotephrites. SBU2 volcanic glasses have a broad range over a more evolved composition, ranging from phonolites to basanites, but with no glasses of more basic basalt-picrobasalt composition (Figure 4a). The volcanic glasses from SBU3 have the broadest range of composition falling into picrobasalt, basalt, basanite, phonotephrite, and phonolite classes (Figure 4a). The SBU4 volcanic glasses have compositions that fall into two groups. One SBU4 group is evolved (>9 wt % alkalis and >52 wt % silica), the other basic (<7 wt % alkalis). Lastly, the SBU5 volcanic glasses of the El Golfo event are found to have highly restricted basic composition (40–45 wt % silica). SBU5 can be divided into two groups comprising 3–4 wt % alkalis basanites and 0.5–2.0 wt % alkali picrobasalts (Figure 4a).

[34] In summary, the subunit glasses from the El Golfo deposit also form discrete compositional fields. Here SBU1 has a broad but relatively basic composition compared to SBU2–4, which have broad but relatively more evolved compositions. Within SBU2–4 distinctions are made whereby SBU2 and SBU4 are more evolved than SBU3, and where SBU3 contains glasses of ultrabasic composition. The last subunit of the El Golfo event (SBU5) has a restricted ultrabasic-basic composition, where the ultrabasic and basanite glasses are comparable to those of SBU1 (Figure 4a).

5.3. Identification of Subunits within Madeira Abyssal Plain Volcaniclastic Turbidites

[35] The northern Madeira Abyssal Plain is fed by the Madeira Channels, which carry turbidity

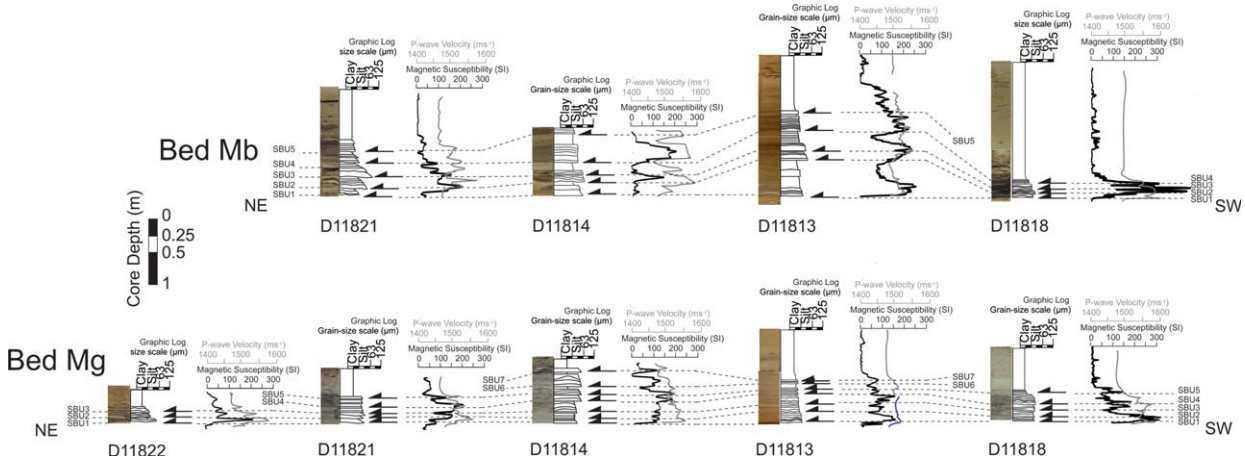

Figure 5. Identified and correlated subunits in the proximal Madeira Abyssal Plain core sites for beds Mb and Mg. Core photograph, visual sedimentary log, *P*-wave velocity and magnetic susceptibility data have been combined to highlight the presence of subunits.

currents from Agadir Basin and offshore Western Canary Islands. Turbidite subunits are generally amalgamated in proximal cores, with erosive removal and/or bypass of the turbidite mud, which is found elsewhere separating the subunit sands in Agadir and distal Madeira Basins. Both *P*-wave velocity and magnetic susceptibility profiles aid verification of the visually identified subunits within these deposits (Figures 5–7). However, unlike in Agadir Basin, the lateral correlation of individual subunits is less certain without further analyses. Thus, these correlations can only be inferred.

[36] Bed Mb has a regular series of five subunits (SBU1–5) identified in D11821, D11814, and D11813 (Figure 5). Bed Mg is more complex with a series of seven potential subunits (SBU1–7) identified in D11814 and D11813, reducing to five at D11821 and D11818, and three at D11822 (Figure 5). The majority of occurrences of bed Mn are as a thin <1 cm silt stringer with a 10–50 cm mudcap. However,

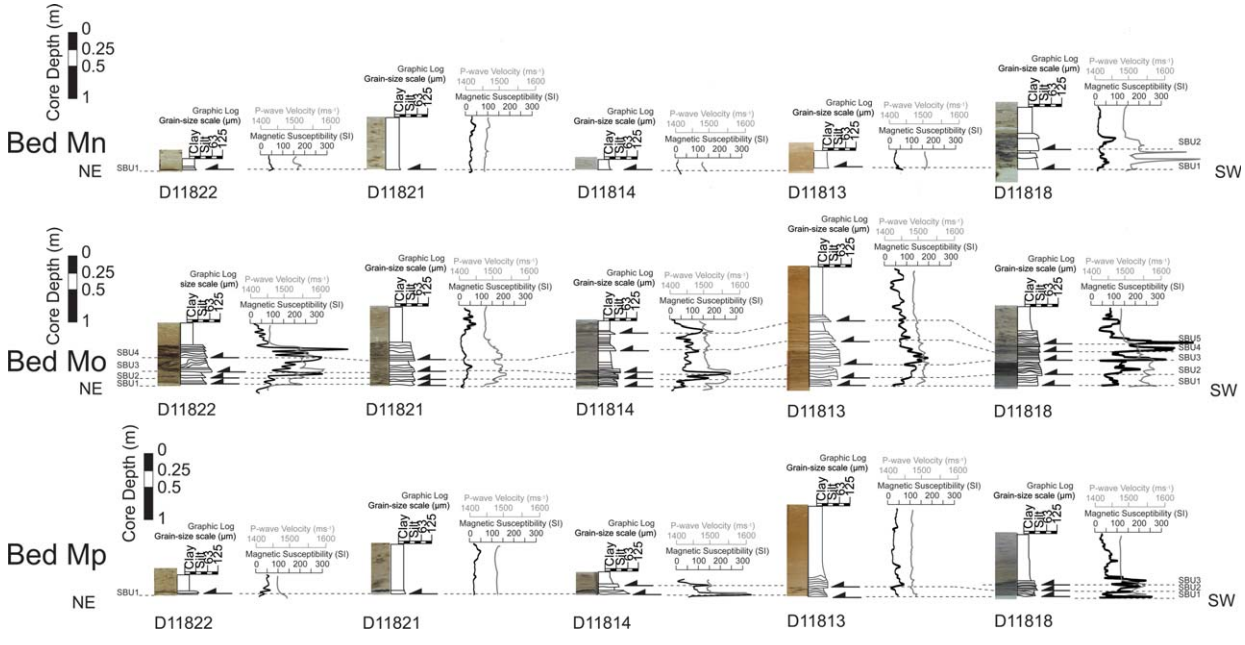

Figure 6. Identified and correlated subunits in the proximal Madeira Abyssal Plain core sites for beds Mn, Mo, and Mp. Core photograph, visual sedimentary log, *P*-wave velocity and magnetic susceptibility data have been combined to highlight the presence of subunits.

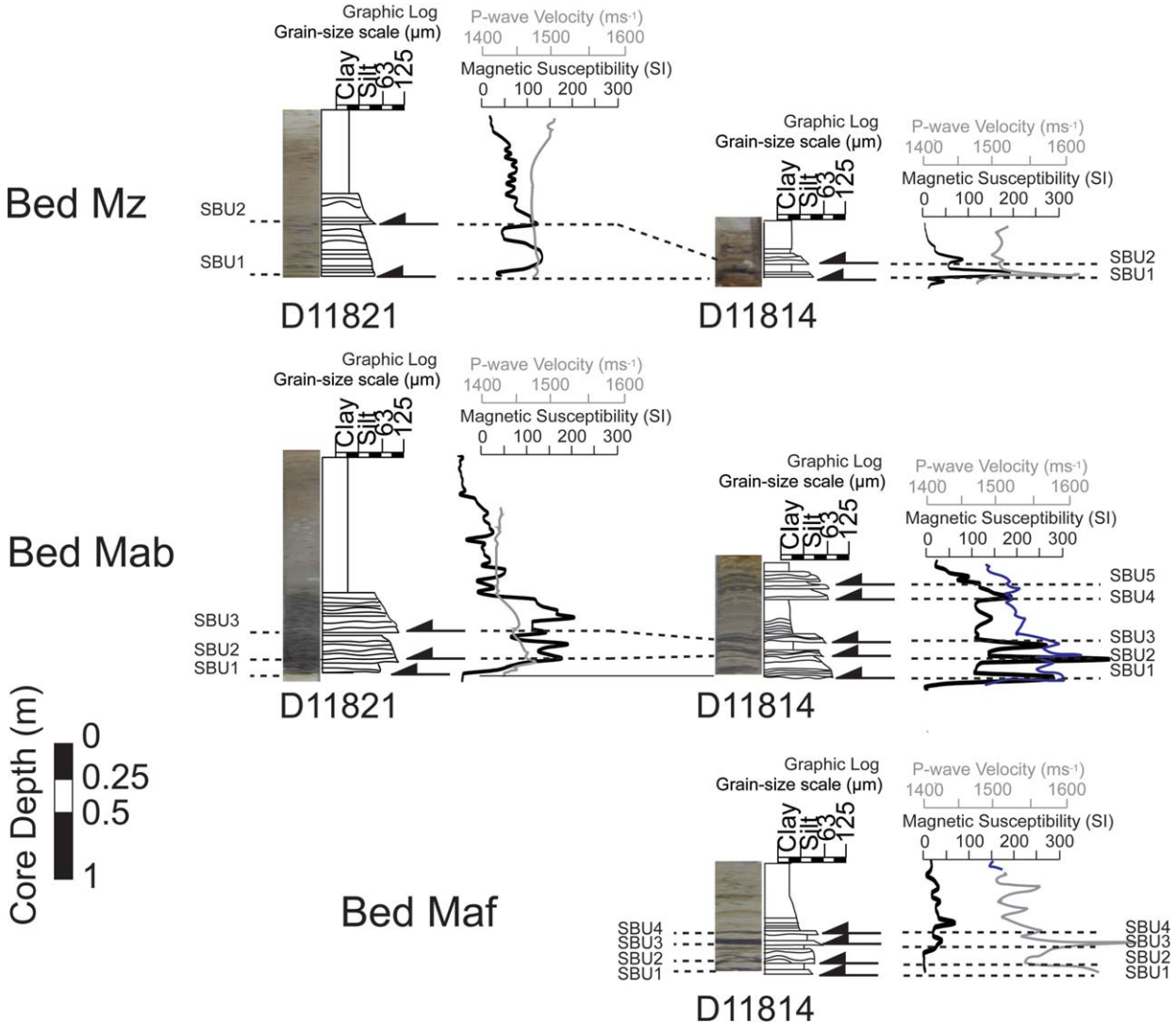

Figure 7. Identified and correlated subunits in the proximal Madeira Abyssal Plain core sites for the examples of beds Mz, Mab, and Maf. Core photograph, visual sedimentary log, *P*-wave velocity and magnetic susceptibility data have been combined to highlight the presence of subunits.

two thick silts are indentified in D11818, suggesting two separate subunits (SBU1–2) (Figure 6). Bed Mo has a complex architecture, with a calcareous-rich basal subunit in D11818 (SBU1), which fines northeast toward D11822. Above this are a series of four well-defined volcanic-rich subunits (SBU2–5), which can be laterally correlated. In contrast to SBU1, SBU3, and SBU4 in bed Mo are coarsest in D11822 (Figure 6). Like Mn, bed Mp predominantly comprises a thin silt stringer and mudcap. However, there are three distinct subunits at sites D11818, D11813, and D11814 (Figure 6).

[37] Of the older deposits, bed Mz has two subunits (SBU1–2) in both D11814 and D11821 (Figure 7). Bed Mab has five subunits in D11814 (SBU1–5), but only three subunits in D11821, where SBU2 and SBU3 are coarsest (Figure 7). Lastly, bed Maf was only recovered at D11814, and was found to comprise four subunits (SBU1–4) (Figure 7).

5.4. Volcanic Glass Geochemistry of Madeira Abyssal Plain Volcaniclastic Turbidite Subunits

[38] Volcanic glasses were analyzed from each subunit from a type example of each volcaniclastic turbidite. These examples were chosen where the subunit record was most complete and the deposits were coarsest. Comparison of results from each subunit also provides an opportunity to identify

compositional hetero-/homogeneities between subunits.

[39] Bed Mb comprises glasses of ultramafic picrobasalt to evolved trachyte-phonolite compositions. The glasses principally fall within the onshore compositional range for El Hierro, although the more evolved glasses have higher silica and alkali components than expected (Figure 8a) [*Le Bas et al*., 1986]. However, the presence of evolved glasses is supported by the original turbidite provenance work by *Pearce and Jarvis* [1992], where the authors' show evolved trachyte glasses with similar compositions.

[40] These results show that the subunits in bed Mb have disparate compositions of volcanic glasses. SBU1 is principally basic in composition restricted to basanites-to-phonotephrites (Figure 8a and Table 2). SBU2 comprises evolved glasses of phonolite and trachyte composition (Figure 8a and Table 2). Both SBU3 and SBU4 have similar compositions, with a dominance of evolved phonolite-trachyte glasses. The SBU3 glasses show increased concentrations of both alkalis and silica, compared to the SBU4 glasses (Figure 8a and Table 2). Furthermore, both SBU3 and SBU4 have glasses of basic composition, with SBU3 restricted to a basalt composition, while the SBU4 basic glasses span basalt to basanite compositions. Lastly, the SBU5 glasses are restricted to basanite-picrobasalt compositions (Figure 8a and Table 2).

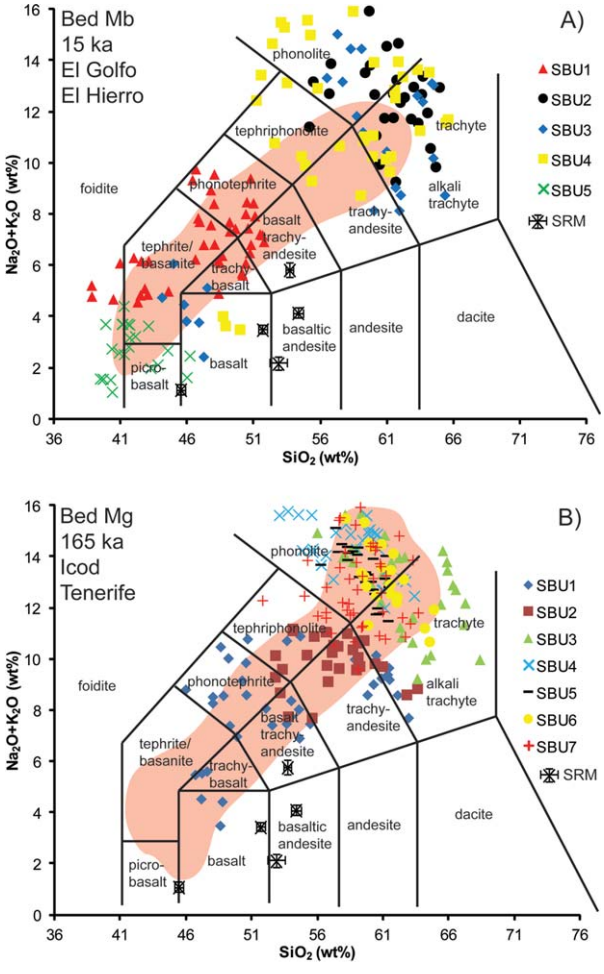

Figure 8. Composition of unaltered volcanic glasses recovered from the subunits of (a) bed Mb from D11814 and (b) bed Mg from D11814. Compositions are plotted on TAS diagrams, showing the disparity between the compositions of the subunits. SRM analyses indicate the error bars as standard deviation. Red transparency represents the onshore whole-rock compositional range from the GEOROCS database.

[41] The volcanic glasses from subunits of the El Golfo turbidite (bed Mb) in Madeira Abyssal Plain are broadly similar to those studied in Agadir Basin (bed A2 in Agadir Basin) (Figure 4a). However, SBU1 and SBU3 lack the ultrabasic picrobasalt glasses in the Madeira Abyssal Plain example. Furthermore, the more basic basanite glasses of SBU2 and SBU4 in the Agadir Basin are absent in the Madeira Abyssal Plain.

[42] Bed Mg volcanic glasses are of alkali basalt to phonolite compositions (Figure 8b). These compositions fall within the onshore compositional field for Tenerife, although the volcanic glasses in the different Mg subunits fall into disparate compositional groups. The initial subunits (SBU1 and SBU2) are the most basic with basalt-to-tephriphonolite compositions (Figure 8b and Table 2). There are a greater number of more evolved tephriphonolite to trachy-andesite glasses in SBU2, compared to SBU1. SBU3 contains amongst the most evolved volcanic glasses, principally trachytes (Figure 8b and Table 2). SBU4 is predominately represented by phonolites with generally high-alkali content. SBU5 and SBU6 have broadly similar glass compositions, being composed of evolved phonolite-trachytes. However, SBU5 has a greater proportion of lower silica phonolites than SBU6 (Figure 8b and Table 2). Lastly, SBU7 is composed of glasses spanning all the compositions present in SBU4, SBU5 and SBU6, but also comprises glasses unique to this subunit (Figure 8b and Table 2).

[43] The Icod event bed is represented by bed Mg in the Madeira Abyssal Plain and bed A14 in Agadir Basin. A previous study examined volcanic glasses from Icod subunit divisions at a proximal site on the southern flank of the Selvagen Islands (site JC27/02) [*Hunt et al*., 2011]. The results of this previous study are comparable to data collected

Table 2. Summary Table of SEM EDS Analyses of Volcanic Glasses From Subunits of Volcaniclastic Beds From the Madeira Abyssal Plain

Bed	SBU1	SBU2	SBU3	SBU4	SBU5	SBU6	SBU7
Mb	Basanites, phonotephrites ad basalt trachy-andesites. 39–52 wt % SiO_2 and 4.5–10 wt % alkalis.	One cluster of evolved phonolite-trachytes. 55–65 wt % SiO_2 and 9–16 wt % alkalis.	Two clusters of phonolite-to-trachytes and basanites. Basic cluster has 44–47.5 SiO_2 and 3.7–6.1 wt % alkalis. Evolved cluster has 55.5–65.5 wt % SiO_2 and 8–15 wt % alkalis.	One predominant cluster of evolved phonolite-trachytes, and one minor basic cluster of basalt composition. Evolved cluster 51–65.5 wt % SiO_2 and 8.5–16 wt % alkalis. Basic cluster 48.5–50 wt % SiO_2 and 3.5–4.0 wt % alkalis.	One basic cluster of picrobasalt to basanite composition. 39.5–46 wt % SiO_2 and 1–4.5 wt % alkalis.	N/A	N/A
Mg	Compositions cover basalts to tephriphonolites. Two basic clusters of 46–55.5 wt % SiO_2 and 3.5–50.5 wt % alkalis, and 59–63 wt % SiO_2 and 7.5–10 wt % alkalis.	Tephriphonolite-to-trachy-andesite composition. SiO_2 of 52.5–63.5 wt % and 7.5–11.5 wt % alkalis.	Trachytes with minor phonolites. 57.5–67.5 wt % SiO_2 and 10–16 wt % alkalis.	Predominantly phonolites. 53–63 wt % SiO_2 and 12.5–16 wt % alkalis.	Phonolite composition with 56–61.5 wt % SiO_2 and 11.5–15.5 wt % alkalis.	Phonolite composition with 57.5–64.5 wt % SiO_2 and 10.5–15.5 wt % alkalis.	Broad phonolite-trachyte composition. With 12.5–64 wt % SiO_2 and 10.5–16 wt % alkalis.
Mn	Two clusters of picrobasalt and trachy-andesite composition. 40.5–44 wt % SiO_2 and 1.8–4.0 wt % alkalis, and 52–53 wt % SiO_2 and 7.2–8.6 wt % alkalis.	One broad cluster of basanite to tephriphonolite. 43.5–53.6 wt % SiO_2 and 4.1–10.7 wt % alkalis.	N/A	N/A	N/A	N/A	N/A
Mo	Two clusters. One of basanites-basalts at 45.5–51.2 wt % SiO_2 and 1.8–7.8 wt % alkalis. Also a group of tephriphonolites, trachytes and phonolites at 50.2–64 wt % SiO_2 and 10–15.2 wt % alkalis.	One group of tephriphonolites-phonolites Composition of 49.5–61.5 wt % SiO_2 and 9–15 wt % alkalis.	Two groups of basanites (42.5–45.8 wt % SiO_2 and 3.2–4 wt % alkalis) and phonolites (50–59.5 wt % SiO_2 and 9–13.7 wt % alkalis.	Comprises a group of phonolites, trachytes and tephriphonolites (50.6–64.7 wt % SiO_2 and 9.2–15 wt % alkalis) and a group of minor trachybasalts (47.5–48.5 wt % SiO_2 and 5.4–6.3 wt % alkalis).	Comprises a group of phonolites, trachytes and tephriphonolites (50.6–64.7 wt % SiO_2 and 9.2–15 wt % alkalis) and a group of minor basalts (45.5–51 wt % SiO_2 and 3.1–6.3 wt % alkalis).	N/A	N/A
Mp	Two clusters. One tephriphonolite-phonolite at 54–61.8 wt % SiO_2 and 8.5–14.5 wt % alkalis. Another basanite group at 43–44 wt % SiO_2 and 3.9–4.7 wt % alkalis.	Two clusters. One phonolite-tephriphonolite at 54–54.6 wt % SiO_2 and 11.1–13.4 wt % alkalis. Another basanite group at 43.6–46 wt % SiO_2 and 4.3–11 wt % alkalis	One basanite group with composition of 42–50.7 wt % SiO_2 and 4.8–7.5 wt % alkalis.	N/A	N/A	N/A	N/A
Mz	Two groups comprising phonolites (50.8–56.8 wt % SiO_2 and 12.4–16 wt % alkalis) and basalt trachy-andesites	Two groups of tephriphonolites (54.8–56.5 wt % SiO_2 wt % and 10.5–11.5 wt % alkalis) and phonolites (58.7–	N/A	N/A	N/A	N/A	N/A

Table 2. (continued)

Bed	SBU1	SBU2	SBU3	SBU4	SBU5	SBU6	SBU7
	(47.3–56.3 wt % SiO_2 and 5.4–9.5 wt % alkalis).	61.2 wt % SiO_2 and 13.5–15.6 wt % alkalis).					
Mab	Two groups comprising basanites (39.5–42.2 wt % SiO_2 and 3.4–6.6 wt % alkalis) and tephriphonolites (46.5–50.5 wt % SiO_2 an 10.5–12 wt % alkalis).	One cluster of basanites to tephriphonolites of 39–53.4 wt % SiO_2 and 6.5–13 wt % alkalis.	Two clusters comprising basalts (40.5–46 SiO_2 and 2.2–4.1 wt % alkalis) and bsalt trachy-andesites to phonotephrites (46–52.7 wt % SiO_2 and 5.5–9.6 wt % alkalis).	One cluster of picrobasalts and basanites of 39–44.8 wt % SiO_2 and 2.2–6.5 wt % alkalis.	Two clusters of basanites at 40.2–43 wt % SiO_2 and 4.7–6.6 wt % alkalis and phonotephrites at 50.5–52 wt % SiO_2 and alkalis at 7.4–8.8 wt %.	N/A	N/A
Maf	Two clusters with one basanite group (44.5–52.4 wt % SiO_2 and 5.8–8 wt % alkalis) and a tephriphonolite-phonolite group (50.1–62.5 wt % SiO_2 and 11.7–15 wt % alkalis.	One group of tephriphonolites, phonolites and trachytes with 52.8–63.3 wt % SiO_2 and 10.4–16 wt % alkalis.	One cluster of basanites to phonotephrites comprising 40.1–53.8 wt % SiO_2 and 3.6–8.8 wt % alkalis.	One group of basalts to phonolits at 46.1–60 wt % SiO_2 and 5.1–13.4 wt % alkalis.	N/A	N/A	N/A

from both Agadir Basin and Madeira Abyssal Plain sites (Figure 4b). However, the most basic basanite and basalt glasses appear to be absent compared to site JC27/02 of *Hunt et al*. [2011].

[44] Bed Mn represents the next volumetrically significant volcaniclastic turbidite in the Madeira Abyssal Plain stratigraphy, which is from La Palma [*Hunt et al*., 2013]. Overall, evolved glasses with >53 wt % SiO_2 are absent. The glasses principally range from picrobasalts to low-alkali tephriphonolites (Figure 9a and Table 2). SBU1 is composed of picrobasaltic glasses with some phonotephrite to basalt trachy-andesite glasses. The SBU2 glasses have a composition different to those of SBU1, comprising mainly basanites, phonotephrites and tephriphonolites (Figure 9a and Table 2).

[45] Five subunits are identified in Bed Mo (Figure 9b and Table 2). The overall glass compositional range is evolved, corresponding to the onshore compositional field for Tenerife (Figure 9b and Table 2). The glasses from SBU1 have two compositions of basic basalt-basanites and tephriphonolite-phonolites (Figure 9b and Table 2). SBU2 comprises evolved glasses, with a small number of phonotephrite-tephriphonolite glasses, but is predominantly composed of high-silica phonolites. SBU3 comprises phonolite and trachyte glasses, but also has a minor group of basalt-basanite glasses (Figure 9b and Table 2). SBU4 has a complex composition of volcanic glasses, with a low-silica phonolite group, a low-alkali tephriphonolite group, a high-alkali trachyte group and a confined group of basanite to trachy-basalt glasses (Figure 9b and Table 2). Finally, the SBU5 glasses cover compositions of all the glasses recovered from the previous Mo subunits (Figure 9b and Table 2).

[46] Bed Mp contains three subunits with an overall composition spanning picrobasalts to phonolites (Figure 9c and Table 2). These compositions are similar to the volcanic glasses analyzed from bed Mb from El Hierro. The SBU1 glasses have two compositional groups of evolved tephriphonolites and phonolite-trachytes and basanites (Figure 9c and Table 2). The SBU2 glasses comprise a group of ultramafic picrobasalts and basanites, and a group of tephroiphonolite-phonolites (Figure 9c and Table 2). The SBU3 glasses represent alkali basanites, without any evidence of evolved glasses (Figure 9c and Table 2).

[47] Bed Mz lacks glasses of basic composition, being instead composed predominantly of evolved volcanic glasses, supporting a Tenerife provenance. The SBU1 glasses have compositions spanning basanites to phonolites (Figure 10a and Table 2).

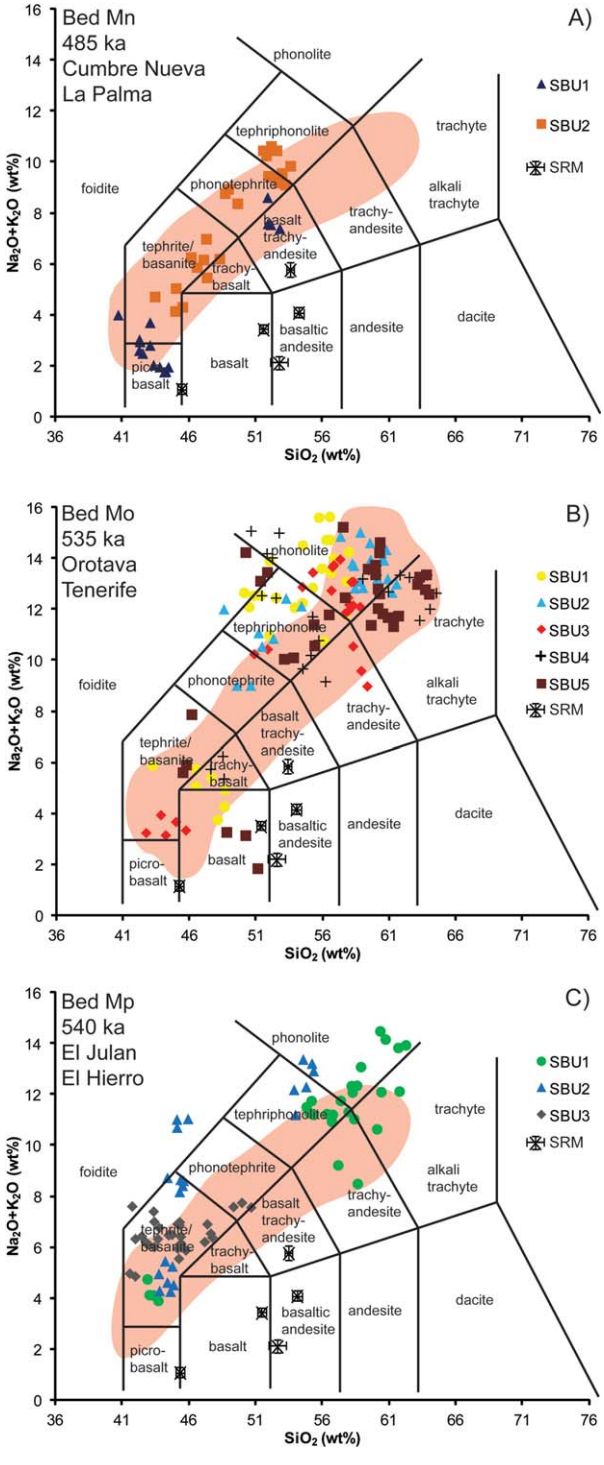

Figure 9. Composition of unaltered volcanic glasses recovered from the subunits of (a) bed Mn from D11818, (b) bed Mo from D11818, and (c) bed Mp from D11818. Compositions are plotted on TAS diagrams, showing the disparity between the compositions of the subunits. SRM analyses indicate the error bars as standard deviation. Red transparency represents the onshore whole-rock compositional range from the GEOROCS database.

Due to a reduced number of >90 μm grains and high numbers of altered grains, there are only 20 measurements taken of glasses from SBU2 (Figure 10a and Table 2).

[48] The bed Mab deposit has five subunits, and the overall glass compositional range lies within that expected of El Hierro. SBU1 glasses cover a range from basic picrobasalts to tephriphonolites (Figure 10b and Table 2). SBU2 glasses have compositions from alkalis basanites to phonolites, and no glasses with compositions <5 wt % alkalis (Figure 10b and Table 2). In comparison, SBU3 comprise glasses with two groups limited to <8–9 wt % alkalis basanites, one being low alkalis and silica, and the other being higher alkalis and silica (Figure 10b and Table 2). The SBU4 glasses have a restricted composition of low-alkali basanites and picrobasalts (Figure 10b and Table 2). Lastly, the SBU5 components represent glasses of basanite composition.

[49] Bed Maf overall comprises predominantly evolved volcanic glasses >46 wt % SiO_2, and lies within the compositional range associated with Tenerife (Figure 10c and Table 2). Here, SBU1 glasses range from alkali basanites to phonolites (Figure 10c and Table 2). SBU2 glasses are evolved with tephriphonolite, phonolite and trachyte compositions (Figure 10c and Table 2). SBU3 contains glasses of basanite and phonotephrite compositions. Finally, the SBU4 glasses cover a range of compositions from high-silica basanites to phonolites (Figure 10c and Table 2).

5.5. Mineral Alteration in Late Quaternary Madeira Abyssal Plain Volcaniclastic Turbidites

[50] Geochemical analyses were conducted on unaltered volcanic glasses. SEM imagery has enabled identification of volcanic glasses that have undergone alteration. A common alteration fabric is the generation of clay minerals and iron-manganese oxides on the surface of the volcanic glasses and lithics (Figure 11). A second fabric is replacement by iron pyrite (Figure 11). These altered grains are present in all the volcaniclastic turbidites studied in the Madeira Abyssal Plain.

6. Discussion

6.1. Subunit Facies Identification in Volcaniclastic Turbidites

[51] Subunits represent the deposits from a series of separate turbidity currents, closely related in

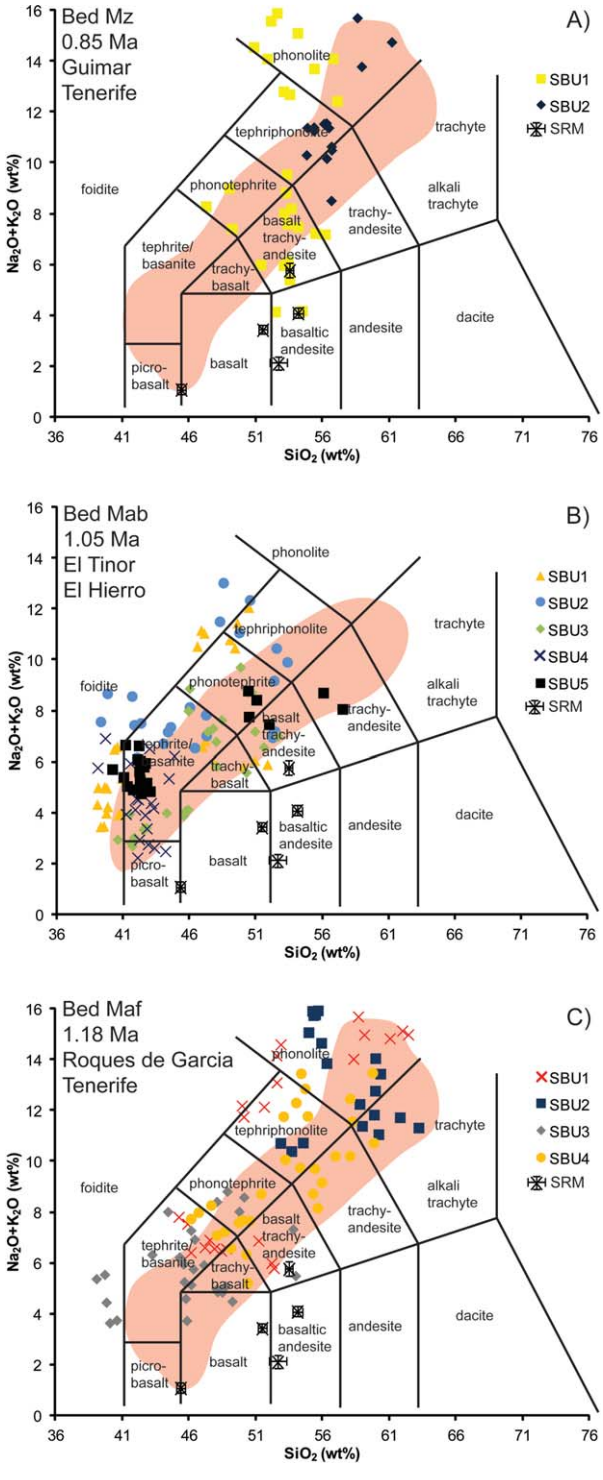

Figure 10. Composition of unaltered volcanic glasses recovered from the subunits of (a) bed Mz from D11814, (b) bed Mab from D11814, and (c) bed Maf from D11814. Compositions are plotted on TAS diagrams, showing the disparity between the compositions of the subunits. SRM analyses indicate the error bars as standard deviation. Red transparency represents the onshore whole-rock compositional range from the GEOROCS database.

time, that together form a single event bed composed of multiple fining-upward turbidite sands and muds. The subunits are characterized by a sharp, sometimes erosive, base with an increase in grain-size above, and with lithic- and carbonate-rich basal compositions. The coarser units can be separated by a turbidite mud or may be amalgamated. These subunits can be correlated over distances greater than 50 km. Indeed the subunits of both the Icod and El Golfo deposits can be regularly correlated over 300 km through Agadir Basin (Figures 2).

6.2. Comparison of Results between Depocentres and the Origin of Subunits

[52] The origin of the subunits can be from flow reflections off topography, flow splitting through channels, synchronous failures from multiple provenances, or from multistage failures at a single source. Determining the origin has implications for the failure and emplacement dynamics of the source landslide. The consistency of the volcanic glass compositions related to a specific island can rule out multiple simultaneous sources (Figures 4 and 8–10). The lack of evidence from onshore and submarine debris apron studies for closely dated events also implies that multiple simultaneous sources are unlikely [*Masson et al*., 2002]. There is no complex channel system feeding Agadir Basin from the Western Canary Islands, thus production of subunits due to flows exiting channels at different times can be ruled out [*Hunt et al*., 2011]. Furthermore, within Agadir Basin a combination of grain-size and geophysical data ruled out flow reflection as the origin of the subunits in the Icod deposit [*Hunt et al*., 2011].

[53] A multistage landslide origin for the Icod landslide was confirmed from analysis of the subunit volcanic glasses from the proximal Icod deposit [*Hunt et al*., 2011]. Geochemical analyses of glasses from subunits of the Icod deposit from Agadir Basin (bed A14) presented in this paper confirm a multistage failure origin (Figure 4b). Indeed, the analysis of glasses from each subunit from Agadir Basin (CD166/27) is consistent with those examined from the proximal site (JC27/02) of the *Hunt et al*. [2011] study. This consistency shows that the seven subunits identified in the Icod deposit can be correlated over distances >300 km, further supporting a multistage failure.

[54] Previously, *Hunt et al*. [2011] stated that analysis of the deposits in the more distal Madeira Abyssal Plain was complicated by the Madeira Channels that feed the Madeira Abyssal Plain

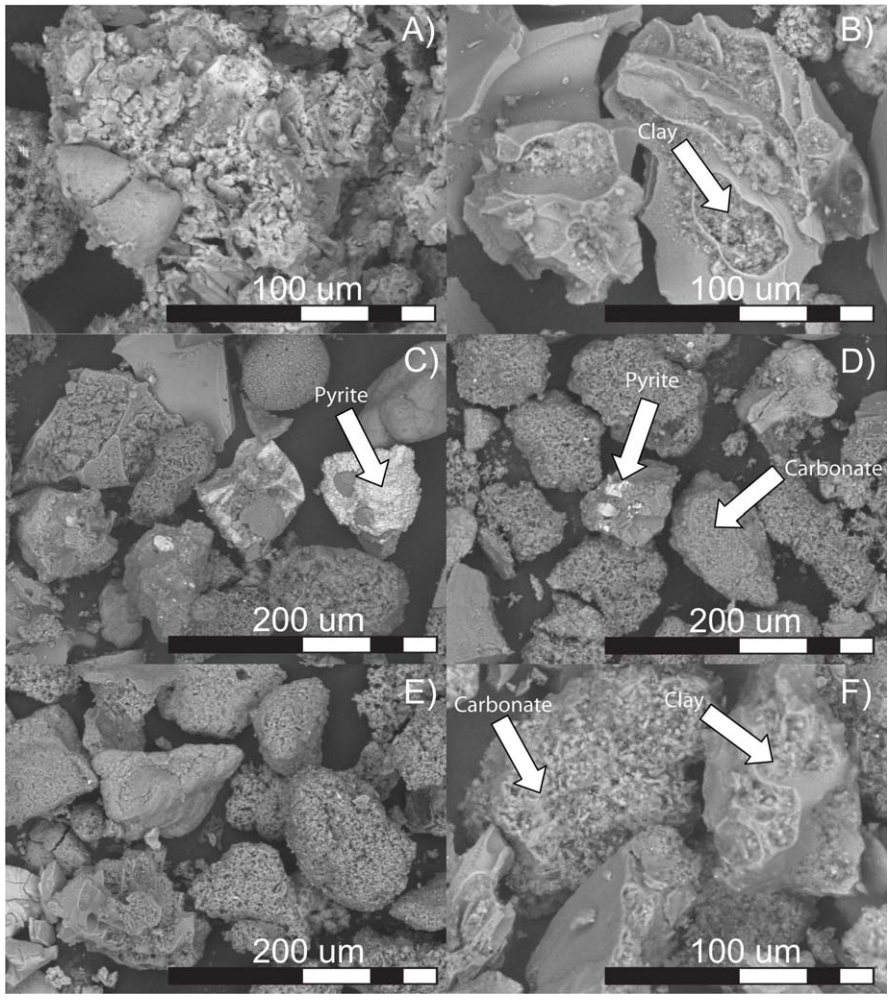

Figure 11. SEM images of altered volcanic glasses and lithics from volcaniclastic turbidites in the Madeira Abyssal Plain, (a) bed Mn, (b) bed Mo, (c) bed Mp, (d) bed Mz, (e) bed Mab, and (f) bed Maf. Alteration is manifested by clay mineral growth on the grain surface and pyrite replacement of the grain.

from Agadir Basin. Theoretically, flows exiting the multiple channels at different times could generate the vertically stacked subunit facies. However, evidence suggests that flows travelling from Agadir Basin to Madeira Abyssal Plain may be accelerated within, but were not confined by, the channels [*Stevenson et al.*, 2013]. Therefore the initial sediment gravity flow may not be split by flowing through different channels.

[55] The composition of the Icod subunits within the Madeira Abyssal Plain (bed Mg) are consistent with those from the Agadir Basin (Figures 4b and 8b). This indicates that the subunits can be reliably correlated from the Agadir Basin to the Madeira Abyssal Plain, ruling out possible effects due to channelized flows and flow reflection, and further supporting a multistage failure origin. The differing compositions of the El Golfo subunit glasses in Agadir Basin (bed A2) also support a multistage failure mechanism. The subunit glass compositions of the El Golfo deposit in the Madeira Abyssal Plain (bed Mb) are also consistent with the subunit glass compositions within Agadir Basin (Figures 4a and 8a). This further demonstrates that the El Golfo subunits can also be correlated between the Agadir Basin and Madeira Abyssal Plain, again supporting multistage failure.

[56] The events responsible for the older Madeira Abyssal Plain volcaniclastic deposits (beds Mn, Mo, Mp, Mz, Mab and Maf) have not been recovered from the thicker Agadir Basin sequence due to lack of core penetration to required depths. The aforementioned consistencies between the El Golfo and Icod subunits from both depocentres imply the subunits within the older Madeira Abyssal Plain deposits likely represent multistage

failures. The geochemistry of the volcanic glasses from the subunits of beds Mn, Mo, Mp, Mz, Mab, and Maf further support the theory that subunits represent multistage failures. The volcanic glasses of the subunits have subtly different compositions from each other (Figures 9 and 10; Table 2). This implies that each subunit potentially represents an individual discrete failure, and is not the product of flow reflection or flow splitting through channels, which would otherwise have near-identical glass compositions.

6.3. Insight into Origin of Volcanic Glasses from Subunits

[57] The compositions of the subunit glasses may be able to demonstrate which particular formations, or at least components of the flank, are incorporated into the failures. El Hierro has a simplistic stratigraphy. Bed Mb (15 ka) has Recent Series glasses in all subunits, except SBU2 and only marginally in SBU4, while SBU5 only comprises Recent Series compositions (Figures 4a and 8a; Table 3). SBU2, 3, and 4 all contain phonolite, trachyte, and tephriphonolite glasses from the Intermediate Series, where SBU3 and 4 contain Basal Series basalts (Figures 4a and 8a; Table 3). Bed Mp lack glasses of the Basal Series which indicate that the failures are relatively shallow. However, while all three subunits comprise basanites and tephrites of the Intermediate Series, only SBU1 and SBU2 have evolved glasses (Figure 9c; Table 3). Bed Mab has five subunits, of which SBU1, SBU2, and SBU5 have specific compositions comparable to Intermediate Series; however, SBU3 and SBU4 also potentially have Basal Series glasses. In this case the later failures of Mab may excavate the deeper sections of the flank (Figure 10b; Table 3).

[58] Bed Mn of La Palma provenance has two subunits. SBU1 of bed Mn has picrobasaltic glasses associated with Basal Complex, while SBU2 glasses are more evolved and potentially related to Taburiente and Cumbre Vieja complexes (Figure 9a; Table 3). This possibly indicates a retrogressive failure.

[59] Those landslides from Tenerife, including beds Mg, Mo, Mz, and Maf have complex associations. The Icod landslide, represented by bed Mg, has initial failures (SBU1–2) comprising glasses of basic composition of either early Cycle III (Canadas III volcano) or from Teno and Anaga massifs (Figures 4b and 8b; Table 3). The upper failures (SBU3–6) comprise glasses from Saltero, Arico, El Rio and Caldera del Rey units, but also higher amounts of glasses from La Mareta, Poris and Wavy Deposit units of the Canadas III cycle. In addition SBU7 only has El Abrigo glasses present (Figures 4b and 8b; Table 3). The strata evacuated during the Icod landslide may indicate a retrogressive failure [*Hunt et al*., 2001].

[60] Bed Mo, representing the La Orotava landslide, contains evolved high-silica phonolites and trachytes similar to those of Saltadero, Arico, Abades and Granadilla units (Figure 9b and Table 3). Although SBU4 and 5 comprise glasses most similar to Granadilla compositions. Bed Mz only has two subunits, which cannot be directly compared to potential onshore strata (Figure 10a and Table 3). Bed Maf has four subunits, of which SBU1 is bimodal, SBU2 comprises only evolved glasses of Cycle I of Canadas III volcano, SBU3 comprises only basanites to phonotephrites of Cycle I, and SBU4 comprises a broad range of phonotephrites to phonolites potentially related to Cycle I of Canadas III (Figure 10cand Table 3).

6.4. Alternative Origins of the Variation in the Volcanic Glass Compositions

[61] The variations in the composition of the volcanic glasses between deposit subunits are used to support a multistage failure. The variations between the subunit glasses in particular beds are suggested to represent subtly different island flank strata failed during each failure stage. Alternative origins for these differences include: different pathways and erosion at source, different pathways and erosion along the turbidity current pathway, and hydraulic separation along the flow pathway.

[62] First, the avalanche lobes are seen to predominantly overlap suggesting that different pathways in the proximal setting are minimal [*Masson et al*., 2002]. Although erosion occurs in the proximal setting, the seafloor sediment is predominantly carbonate hemipelagite, therefore erosive addition of enough volcaniclastic material to provide glasses of different compositions within the populations measured is unlikely [*Hunt et al*., 2011]. The turbidity currents are principally nonerosive distally [*Weaver and Thomson*, 1993; *Weaver*, 1994; *Hunt et al*., 2011], and there are not multiple pathways distally from the island flanks (Figure 1). Although the Madeira Channels are present between Agadir Basin and Madeira Abyssal Plain, *Stevenson et al*. [2013] show that firstly the flows are only marginally accelerated within the channel regions, and secondly that flows are nonerosive within them. Therefore, the effects of different flow

Table 3. Summary Table of Volcanic Glass Compositions From Subunits of Volcaniclastic Beds From the Madeira Abyssal Plain[a]

Bed	SBU1	SBU2	SBU3	SBU4	SBU5	SBU6	SBU7
Mb	Recent Series and Intermediate Series tephrites and phonotephrites.	SBU3 also contain Recent Series, but only SBU2, 3, and 4 contain the evolved phonolites, trachytes and tephrites of the Intermediate Series. SBU3 and SBU4 also only divisions to contain glasses potentially from Basal Series.			Only Recent Series represented.	N/A	N/A
Mg	SBU1 and 2 do not contain any phonolites or trachytes that are the later cycle 2 or 3 ignimbrites of the Canadas III series. There are basalts to tephriphonolites that are either of Canadas III basalt series or those from Anaga or Teno massifs.		Saltdero, Arico, El Rio and Caldera del Rey phonolites and tephrites.	SBU4, 5, and 6 contain a range of glasses from Saltero, Arico, El Rio and Caldera del Rey units, but also higher amounts of glasses from La Mareta, Poris and Wavy Deposit units of the Canadas III cycle.			Contains glasses from La Mareta and Poris units, but predominantly of El Abrigo unit.
Mn	Contains picrobasalts associated with Basal Complex and Seamount Phase.	Tephriphonolites of Cumbre Vieja. Tephrites from Cumbre Vieja or Taburiente. Phonotephrites from Bejenado.	N/A	N/A	N/A	N/A	N/A
Mo	High alkali but low silica glasses and a cluster of basalts.	All contain evolved high-silica phonolites and trachytes that are similar to those of Saltadero, Arico, Abades and Granadilla units. With SBU4 and 5 having glasses most similar to Granadilla compositions. SBU3, 4, and 5 have variable content of basic glasses possibly of Cycle II mafics or older Teno or Anaga massifs. SBU2 only has tephriphonolite to phonolite composition.				N/A	N/A
Mp	SBU1, 2, and 3 all have glasses from the basanites and tephrites of the Intermediate Series. SBU1 and 2 have glasses from evolved compositions of the Intermediate Series, not SBU3. None have glasses of the Basal Series or Recent Series.			N/A	N/A	N/A	N/A
Mz	Phonolites and basalt trachy-andesites possibly from older rift arm activity. Also evolved phonolites.	Tephriphonlites present.	N/A	N/A	N/A	N/A	N/A
Mab	Only basanite and tephriphonolites glasses of Intermediate Series.	Only alkali-rich tephrites and tephriphonolites of Intermediate series.	SBU3 and 4 have compositions potentially of the Basal Series. SBU3 then only has phonotephrites of Intermediate Series, while SBU4 only has low-silica basanite-tephrites of Intermediate Series.		Very specific composition of basanite-tephrites associated with Intermediate Series.	N/A	N/A
Maf	Bimodal composition. Basic glasses possibly related to Cycle I mafics of the Canadas III edifice or older Anaga or Teno massifs, while phonolites also present.	Only evolved phonolites and trachytes present related to Cycle I of Canadas III.	Comprising only basanites to phonotephrites of Cycle I.	A broad range of phonotephrites to phonolites related to Cycle I of Canadas III.	N/A	N/A	N/A

[a]Comparisons are related to data compiled from GeoRocs Max Plank database, *Pellicer et al.* [1979], *Staudigel and Schmincke* [1984], *Bryan et al.* [2002], *Huertas et al.* [2002], *Galipp et al.* [2006] and *Praegel and Holm* [1979].

pathways and erosive behavior both proximally and distally can be discounted as a mechanism generating the variations in the subunit glass compositions.

[63] Hydraulic separation of grains to produce these variations in glass compositions is a potential issue, for example ultrabasic glasses in the more proximal locations of both El Golfo and Icod deposits are missing at distal sites. However, grains of a particular grain size (90–125 μm) and morphology were chosen to specifically reduce the effects of this [*Hunt et al*., 2011]. The present study also shows that there are consistencies within the deposits throughout the flow pathway, as seen between the El Golfo and Icod subunits in the Agadir Basin and Madeira Abyssal Plain, and in comparison to the Icod deposit recorded by *Hunt et al*. [2011]. These similarities between particular subunits at different sites imply that hydraulic sorting is minimal in controlling the overall composition of the assemblage of respective subunits. Multistage failure of a heterogeneous source is the primary origin of the differences in the subunit glass compositions, especially the evolved phonolite-trachyte compositions, of a particular bed.

6.5. Multistage Landslide Mechanisms and Implication for Tsunamigenesis

[64] Deposit volumes in the Madeira Abyssal Plain provide a minimum estimate of the total volume involved in the failure [*Hunt et al*., 2013]. Total deposit volumes (i.e., summing all subunits in each event bed) range from 50–150 km^3 in the Madeira Abyssal Plain [*Hunt et al*., 2013]. An additional 10–150 km^3 could potentially be deposited in Agadir Basin, based on the two beds sampled to date [*Frenz et al*., 2009; *Hunt et al*., 2011]. Adding proximal debris avalanche volumes of 50–200 km^3 [*Masson et al*., 2002], the total landslide volumes, including sediment remobilized from the island flanks, do not exceed 350 km^{-3}, and are certainly not the 500 km^3 used in the models of the potential future Cumbre Nueva landslide [*Ward and Day*, 2001; *Gisler et al*., 2006].

[65] The identification of multistage failures for the 1.5 Ma-to-recent Canary Island landslides has wider implications. The volume of a landslide is a primary control on the magnitude of the associated tsunami [*Murty*, 2003]. Multistage collapses serve to divide the total landslide volume among several smaller events. Multistage collapse with sufficient lag time would significantly reduce tsunami magnitude (scale of minutes), as shown by modeling of the Güímar landslide as a single and multistage failure [*Giachetti et al*., 2011]. Having shown that the eight large-volume Canary Island failures in the last 1.5 Ma were multistage, it is likely that subsequent failures will also be multistage. However, even within a multistage landslide scenario, given the large volumes of the past events, associated tsunamis could still be very damaging [*Paris et al*., 2011; *Abadi et al*., 2012].

[66] As shown by *Hunt et al*. [2011], the relative proportions of landslide material derived from the island flank also poses an important control on tsunamigenesis [*Fine et al*., 2003]. They demonstrated that altered volcanic glasses and elevated carbonate content in the basal subunits of the Icod event bed represent initial stages of failure with a significant submarine component. The presence of altered glasses and lithics in all the deposits examined in this study (Figure 11), coupled with high-basal carbonate contents, imply that these landslides also had a submarine component. This is further supported by landslides having volumes in excess of the onshore scar, requiring a submarine component for mass balance [*Hunt et al*., 2013]. Although the submarine portion of the failure would contribute to tsunamigenesis, this contribution would be less than that of a purely subaerial failure [*Watt et al*., 2012].

7. Conclusions

[67] Turbidites in the Madeira Abyssal Plain record the eight most recent large-volume (50–350 km^3) Canary Island landslides. This turbidite record serves to help date landslides and preserves key information concerning the failure mechanism of the landslide. Each large-volume event bed comprises a series of multiple fining-upward turbidite sands and muds, known as subunits. Comparison of the geochemistry of volcanic glasses from the subunits indicates that they have different compositions. Thus, each subunit represents a separate failure within a multistage landslide. This has implications for the tsunamigensis of volcanic island landslides, since multistage failures will likely reduce the size of individual tsunami waves. Furthermore, the basal subunits typically contain altered volcanic glasses and high carbonate content indicative of materials failed from the submarine flanks of the islands. The incorporation of submarine flank sectors into the landslides is also important, since this also acts to further reduce tsunamigenesis. However, although reduced in volume due to multistage failure mechanism, the

volume of these separate failures are still substantial (10–100 km^3) and capable of causing significant tsunamis near to source.

Acknowledgments

[68] The authors would like to thank the scientists and crew that worked on the D108 and CD166 cruises which collected the piston cores used in this study. JEH would like to acknowledge the PhD funding from Marine Geoscience Group at NOCS that aided completion of this work.

References

Abadi, S. M., J. C. Harris, S. T. Grilli, and R. Fabre (2012), Numerical modeling of tsunami waves generated by the flank collapse of the Cumbre Vieja Volcano (La Palma, Canary Islands): Tsunami source and near field effects, *J. Geophys. Res.*, *117*, C05030, doi:10.1029/2011JC007646.

Acosta, J., E. Uchupi, A. Muñoz, P. Herranz, C. Palomo, M. Ballesteros, and ZEE Working Group (2003), Geologic evolution of the Canary Islands of Lanzarote, Fuerteventura, Gran Canaria and La Gomera and comparison of the landslides at these islands with those at Tenerife, La Palma and El Hierro, *Mar. Geophys. Res.*, *24*, 1–40, doi:10.1007/s11001-004-1513-3.

Ancochea, E., J. M. Fúster, E. Ibarrola, A. Cendrero, J. Coello, F. Hernan, J. M. Cantagrel, and C. Jamond (1990), Volcanic evolution of the island of Tenerife (Canary Islands) in light of new K-Ar data, *J. Volcanol. Geotherm. Res.*, *44*, 231–249, doi:10.1016/0377-0273(90)90019-C.

Ancochea, E., M. J. Huertas, J. M. Cantagrel, J. Coello, J. M. Füster, N. O. Arnaud, and E. Ibarraola (1999), Evolution of the Cañadas Edifice and its implications for the origin of the Cañadas Caldera (Tenerife, Canary Islands), *J. Volcanol. Geotherm. Res.*, *88*, 177–199.

Bryan, S. E., J. Marti, and M. Leosson, (2002), Petrology and geochemistry of the Bandas del Sur Formation, Las Cañadas Edifice, Tenerife (Canary Islands), *J. Petrol.*, *43*(10), 1815–1856.

Cantagrel, J. M., N. O. Arnaud, E. Ancochea, J. M. Fúster, and M. J. Huertas (1999), Repeated debris avalanches on Tenerife and genesis of Las Cañadas caldera wall (Canary Islands), *Geology*, *27*(8), 739–742.

Carracedo, J. C. (1994), The Canary Islands: An example of structural control on the growth of large oceanic-island volcanoes, *J. Volcanol. Geotherm. Res.*, *60*, 225–241.

Carracedo, J. C. (1999), Growth, structure, instability and collapse of Canarian volcanoes and comparisons with Hawaiian volcanoes, *J. Volcanol. Geotherm. Res.*, *94*, 1–19.

Carracedo, J. C., S. J. Day, H. Guillou, E. Rodríguez Badiola, J. A. Canas, and F. J. Pérez Torrado (1998), Hotspot volcanism close to a passive continental margin: The Canary Islands, *Geol. Mag.*, *135*(5), 591–604.

Carracedo, J. C., S. J. Day, H. Guillou, and F. J. Pérez Torrado (1999), Giant Quaternary landslides in the evolution of La Palma and El Hierro, Canary Islands, *J. Volcanol. Geotherm. Res.*, *94*, 169–190.

Di Roberto, A., M. Rossi, A. Bertagnini, M. P. Marani, M. P., and F. Gamberi (2010), Distal turbidites and tsunamigenic landslides of Stromboli Volcano (Aeolian Islands, Italy), in *International Symposium on Submarine Mass Movements and Their Consequences, Adv. in Nat. and Technol. Hazard Res*., vol. *28*, edited by D. C. Mosher, C. Shipp, L. Moscardelli, J. Claytor, C. Baxter, H. Lee, and R. Urgeles, pp.719–732, Springer, Dordrecht, Netherlands.

Fine, I.V., E.V. Kulikov, R.E. Thomson, and A.B. Rabinovich (2001), Modeling of tsunami generation by submarine and subaerial landslides, *Proceedings International Tsunami Symposium*, Seattle, Washington, 7–10 August, 663.

Fine, I.V., A.B. Rabinovich, R.E. Thomson and E.A. Kulikov (2003), Numerical Modeling of Tsunami Generation by Submarine and Subaerial Landslides, Submarine Landslides and Tsunamis, NATO Science Series, Vol. 21, 69–88.

Fine, I. V., A. B. Rabinovich, R. E. Thomson, and E. A. Kulikov (2003), Numerical modelling of tsunami generation by submarine and subaerial landslides, in *Submarine Landslides and Tsunamis*, edited by A. C. Yalçiner, E. Pelinovsky, and C. E. Synolakis, Kluwer Acad., Neth.

Frenz, M., R. B. Wynn, A. Georgiopoulou, V. B. Bender, G. Hough, D. G. Masson, P. J. Talling, and B. Cronin (2009), Provenance and pathways of late quaternary turbidites in the deep-water Agadir Basin, northwest African margin, *Int. J. Earth Sci.*, *98*(4), 721–733.

Galipp, K., A. Klugel, and T. H. Hansteen (2006), Changing depths of magma fractionation and stagnation during the evolution of an oceanic island volcano: La Palma (Canary Islands), *J. Volcanol. Geotherm. Res.*, *155*, 285–306.

Garcia, M. O. (1996), Turbidites from slope failure of Hawaiian volcanoes, in *Volcano Instability on the Earth and Other Planets, Geol. Soc. Spec. Pub*, vol. *110*, edited by W. J. McGuire, A. P. Jones and J. Neuberg, pp. 281–294, Geol. Soc., London, U. K.

Garcia, M. O., and D. M. Hull (1994), Turbidites from giant Hawaiian landslides: Results from Ocean Drilling Program Site 842, *Geology*, *22*, 159–162.

Gee, M. J. R., A. B. Watts, D. G. Masson, and N. C. Mitchell (2001), Landslides and evolution of El Hierro in the Canary Islands, *Mar. Geol.*, *177*, 271–294.

GEOREM, *Database for Geological and Environmental Reference Materials*, Max-Planck-Gesellschaft. [Available at georem.mpch-mainz.gwdg.de, accessed 23 Apr. 2013]

GEOROC, *Database for Geochemistry of Rocks of the Oceans and Continents*, Max-Planck-gesellschaft. [Available at georoc.mpch-mainz.gwdg.de/georoc, accessed 23 Apr. 2013].

Giachetti, T., R. Paris, K. Kelfoun, and F. J. Pérez-Torrado (2011), Numerical modelling of the tsunami triggered by the Güímar debris avalanche, Tenerife (Canary Islands): Comparison with field-based data, *Mar. Geol.*, *284*, 189–202.

Gisler, G., R. P. Weaver, and M. L. Gittings, (2006), SAGE calculations of the tsunami threat from La Palma, *Sci. Tsunami Hazards*, *24*(4), 288–301.

Guillou, H., J. C. Carracedo, F. Pérez Torrado, and E. Rodríguez Badiola (1996), K-Ar ages and magnetic stratigraphy of a hotspot-induced, fast grown oceanic island: El Hierro, Canary Islands, *J. Volcanol. Geotherm. Res.*, *73*, 141–155.

Harbitz, C. B. (1992), Model simulations of tsunamis generated by the Storegga Slides, *Mar. Geol.*, *105*, 1–21.

Harbitz, C. B., G. Pedersen, and B. Gjevik (1993), Numerical simulations of large water waves due to landslides, *J. Hydraul. Eng.*, *119*(12), 1325–1342, doi:10.1061/(ASCE)0733–9429(1993)119:12(1325).

Harbitz, C. B., F. Løvholt, G. Pedersen, and D. G. Masson (2006), Mechanisms of tsunami generation by submarine landslides: A short review, *Norw. J. Geol.*, *86*, 255–264.

Haugen, K. B., F. Løvholt, and C. B. Harbitz (2005), Fundamental mechanisms for tsunami generation by submarine

flows in idealised geometries, *Mar. Pet. Geol.*, *22*, 209–217, doi:10.1016/j.marpetgeo.2004.10.016.

Hoernle, K. A. J., and H.-U. Schmincke (1993), The role of partial melting in the 15 Ma geochemical evolution of Gran Canaria: A blob model for the Canary Hotspot, *J. Petrol.*, *34*(3), 599–626.

Hoernle, K. A. J., Y.-S. Zhang, and D. Graham (1995), Seismic and geochemical evidence for large-scale mantle upwelling beneath the eastern Atlantic and western and central Europe, *Nature*, *374*, 34–39.

Holcomb, R. T., and R. C. Searle (1991), Large landslides from oceanic volcanoes, *Mar. Geotechnol.*, *10*(1–2), 19–32.

Howe, R. W., and J. Sblendorio-Levy (1998), Calcareous nannofossil biostratigraphy and sediment accumulation of turbidite sequences on the Madeira Abyssal Plain, Sites 950–952, in *Proceedings of the Ocean Drilling Scientific Results*, vol. *157*, edited by P. P. E. Weaver, H.-U. Schmincke, J. V. Firth, and W. Duffield, pp. 501–520, Ocean Drilling Program, Coll. Stn., Tex, doi:10.2973/odp.proc.sr.157.147.1998.

Huertas, M. J., N. O. Arnaud, E. Ancochea, J. M. Cantarel, and J. M. Fúster (2002), 40Ar/39Ar Stratigraphy of pyroclastic units from Cañadas Volcanic Edifice (Tenerife, Canary Islands) and their bearing on the structural evolution, *J. Volcanol. Geotherm. Res.*, *115*, 351–365.

Hunt, J. E., R. B. Wynn, D. G. Masson, P. J. Talling, and D. A. H. Teagle (2011), Sedimentological and geochemical evidence for multistage failure of volcanic island landslides: A case study from Icod landslide on north Tenerife, *Geochem. Geophys. Geosyst.*, *12*, Q12007, doi:10.1029/2011GC003740.

Hunt, J. E., R. B. Wynn, P. J. Talling, and D. G. Masson (2013), Turbidite record of frequency and source of large volume (>100 km^3) Canary Island landslides in the last 1.5 Ma: Implications for landslide triggers and geohazards, *Geochem. Geophys. Geosyst.*, *XX*, doi:10.1002/ggge.20139.

Klitgort, K. D., and H. Schouten (1986), Plate kinematics of the central Atlantic, in *The Geology of North America, vol. M, The Western North Atlantic Region*, edited by P. R. Vogt and B. E. Tucholke, pp. 351–377, Geol. Soc. of Am., Boulder, Colo.

Krastel, S., H.-U. Schmincke, C. L. Jacobs, R. Rihm, T. P. Le Bas, and B. Alibés (2001), Submarine landslides around the Canary Islands, *J. Geophys. Res.*, *106*, 3977–3997.

Labazuy, P. (1996), Recurrent landslide events on the submarine flank of Piton de la Fournaise volcano (Réunion Island), in *Volcano Stability on the Earth and Other Planets, vol. 110*, edited by W. J. McGuire, A. P. Jones, and J. Neuberg, pp. 295–306, Geol. Soc. Spec. Publ., London, U. K.

Le Bas, M. J., R. W. Le Maitre, A. Streckeisen, and B. Zanettin (1986), A chemical classification of volcanic rocks based on total alkali-silica diagram, *J. Petrol.*, *27*(3), 745–750.

Le Bas, T. P., D. G. Masson, R. Holtom, and I. Grevemeyer (2007), Slope failures of the flanks of the southern Cape Verde Islands, in *International Symposium on Submarine Mass Movements and Their Consequences, Adv. in Nat. and Technol. Hazard Res.*, vol. 27, edited by V. Lykousis, D. Sakellariou, and J. Locat, pp. 337–346, Springer, Dordrecht, Netherlands.

Lenát, J.-F., P. Vincent, and P. Bachélery (1989), The offshore continuation of an active basaltic volcano: Piton de la Fournaise (Réunion Island, Indian Ocean); structural and geomorphological interpretation from sea beam mapping, *J. Volcanol. Geotherm. Res.*, *36*(1–3), 1–36.

Lisiecki, L. E., and M. E. Raymo (2005), A Pliocene-Pleistocene stack of 57 globally distributed benthic d18O records, *Paleoceanography*, *20*, PA1003, doi:10.1029/2004PA001071.

Løvholt, F., C. B. Harbitz, and K. B. Haugen (2005), A parametric study of tsunamis generated by submarine slides in the Ormen Lange/Storegga area off western Norway. *Mar. Petrol. Geol.*, *22*(1–2), 219–231, doi:10.1016/j.marpetgeo.2004.10.1017.

Løvholt, F., G. Pedersen, and G. Gisler (2008), Oceanic propagation of a potential tsunami from the La Palma Island. *J. Geophys. Res.*, *113*, C09026, doi:10.1029/2007JC004603.

Mader, C. L. (2001), Modelling the La Palma landslide tsunami, *Sci. Tsunami Hazards*, *19*, 150–170.

Marti, J., and A. Gudmundsson (2000), The Las Cañadas Caldera (Tenerife, Canary Islands): An overlapping collapse caldera generated by magma-chamber migration, *J. Volcanol. Geotherm. Res.*, *103*, 161–173.

Marti, J., J. Mitjavila, and V. Arana (1994), Stratigraphy, structure and geochronology of the La Canadas caldera, Tenerife, Canary Islands, *Geol. Mag.*, *131*, 715–727.

Masson, D. G. (1994), Late Quaternary turbidity current pathways to the Madeira Abyssal Plain and some constraints on turbidity current mechanisms, *Basin Res.*, *6*, 17–33.

Masson, D. G. (1996), Catastrophic collapse of the volcanic island of Hierro 15 ka ago and the history of landslides in the Canaries, *Geology*, *24*, 231–234, doi:10.1130/0091–7613(1996)024<0231:CCOTVI>2.3.CO;2.

Masson, D. G., B. Van Niel, and P. P. E. Weaver (1997), Flow processes and sedimentation deformation in the Canary Debris Flow on the NW African Continental Rise, *Sediment. Geol.*, *110*(3–4), 163–179.

Masson, D. G., A. B. Watts, M. R. J. Gee, R. Urgeles, N. C. Mitchell, T. Le Bas, and M. Canals (2002), Slope failures on the flanks of the western Canary Islands, *Earth Sci. Rev.*, *57*, 1–35.

Masson, D. G., C. B. Harbitz, R. B. Wynn, G. Pedersen, and F. Løvholt (2006), Submarine landslides: Processes, triggers and hazard prediction, *Philos. Trans. R. Soc. A*, *364*, 2009–2039, doi:10.1098/rsta.2006.1810.

Masson, D. G., T. Le Bas, I. Grevemeyer, and W. Weinrebe (2008), Flank collapse and large-scale landsliding in the Cape Verde Islands, off West African, Geochem. *Geophys. Geosyst.*, *9*, Q07015, doi:10.1029/2008GC001983.

McMurtry, G. M., G. J. Fryer, D. R. Tappin, I. P. Wilkinson, M. Williams, J. Fietzke, D. Garbe-Schoenberg, and P. Watts (2004), Megatsunami deposits on Kohala volcano, Hawaii, from flank collapses of Mauna Loa, *Geology*, *32*(9), 741–744.

Moore, J. G., D. A. Clague, R. T. Holcomb, P. W. Lipman, W. R. Normark, and M. E. Torresan (1989), Prodigious submarine landslides on the Hawaiian Ridge, *J. Geophys. Res.*, *94*, 17,465–17,484.

Moore, J. G., W. R. Normark, and R. T. Holcomb (1994), Giant Hawaiian landslides, *Ann. Rev. Earth Planet. Sci.*, *22*, 119–144, doi:10.1146/annurev.ea.22.050194.001003.

Murty, T. S. (2003), Tsunami wave height dependence on landslide volume, *Pure Appl. Geophys.*, *160*(2003), 2147–2153.

Oehler, J. F., P. Labazuy, and J. F. Lénat (2004), Recurrence of major flank landslides during the last 2Ma history of Réunion Island, *Bull. Volcanol.*, *66*(7), 585–598.

Oehler, J. F., J. F. Lénat, and P. Labazuy (2008), Growth and collapse of the Réunion Island volcanoes, *Bull. Volcanol.*, *70*(6), 717–742.

Paris, R., T. Giachetti, J. Chevalier, H. Guillou, and N. Frank (2011), Tsunami deposits in Santiago Island (Cape Verde archipelago) as possible evidence of a massive flank failure of Fogos volcano, *Sediment. Geol.*, *239*(3–4), 129–145.

Pearce, T. J., and I. Jarvis (1992), Composition and provenance of turbidite sands: Late Quaternary, *Madeira Abyssal Plain*, Mar. Geol., *109*, 21–51.

Pellicer, J. M. (1979), Estudio geoquimico del vulcanismo de la isla del Hierro, Archipelago Canario, *Estudios Geol.*, *35*, 15–29.

Praegel, N.-O., and P. M. Holm (2006), Lithospheric contributions to high-MgO basanites from the Cumbre Vieja Volcano, La Palma, Canary Islands and evidence for temporal variations in plume influence, *J. Volcanol. Geotherm. Res.*, *149*, 213–239.

Schmincke, H.-U., A. Klügel, T. H. Hansteen, K. Hoernle, and P. van den Bogaard (1998), Samples from the Jurassic ocean crust beneath Gran Canaria, La Palma and Lanzarote (Canary Islands), *Earth Planet. Sci. Lett.*, *163*(1–4), 343–360.

Staudigel, H., and H.-U. Schmincke (1984), The Pliocene seamount series of La Palma, Canary Islands, *J. Geophys. Res.*, *89*, 11, 195–11,215.

Stevenson, C. J., P. J. Talling, R. B. Wynn, D. G. Masson, J. E. Hunt, M. Frenz, A. Akhemtzhanov, and B. T. Cronin (2013), The flows that left no trace: Very large-volume turbidity currents that bypassed sediment through submarine channels without eroding the sea floor, *Mar. Petrol. Geol.*, *41*, 186–205.

Tinti, S., E. Bortolucci and A. Armigliato (1999), Numerical simulation of the landslide-induced tsunami of 1988 on Vulcano, *Bull. Volcanol.*, *61*(1–2), 121–137, doi:10.1007/s004450050267.

Tinti, S., E. Bortoluci, and C. Romagnoli (2000), Computer simulations of tsunamis due to sector collapse at Stromboli, Italy, *J. Volcanol. Geotherm. Res.*, *96*(1–2), 103–128, doi:10.1016/S0377-0273(99)00138-9.

Trifunac, M. D., and M. I. Todorovska (2002), A note on the differences in tsunami source parameters for submarine slides and earthquakes, *Soil Dyn. Earthquake Eng.*, *22*, 143–155.

Urgeles, R., M. Canals, J. Baraza, B. Alonso, and D. G. Masson (1997), The most recent megaslides on the Canary Islands: The El Golfo avalanche and the Canary Debris flow, *J. Geophys. Res.*, *102*, 20,305–20,323, doi:10.1029/97JB00649.

Urgeles, R., D. G. Masson, M. Canals, A. B. Watts, and T. P. Le Bas (1999), Recurrent large-scale landsliding on the west flank of La Palma, Canary Islands, *J. Geophys. Res.*, *104*, 25,331–25,348.

Urgeles, R., Canals, M., and D. G. Masson, (2001), Flank stability and processes off the western Canary Islands: A review from El Hierro and La Palma, *Sci. Mar.*, *65*, 21–31.

Ward, S. N. (2001), Landslide tsunami, *J. Geophys. Res.*, *106*, 11,201–11,215, doi:10.1029/2000JB900450.

Ward, S. N., and S. J. Day (2001), Cumbre Vieja volcano: Potential collapse and tsunami at La Palma, Canary islands, *Geophys. Res. Lett.*, *28*, 3397–3400, doi:10.1029/2001GL013110.

Ward, S. N., and S. J. Day (2003), Ritter Island Volcano: Lateral collapse and tsunami of 1888, *Geophys. J. Int.*, *154*(3), 891–902.

Watt, S. F. L., et al. (2012), Combinations of volcanic-flank and seafloor-sediment failure offshore Monserrat, and their implications for tsunami generation, *Earth Planet*, *Sci. Lett.*, 319–320, 228–240.

Watts, A. B., and D. G. Masson (1995), A giant landslide on the north flank of Tenerife, Canary Islands, *J. Geophys. Res.*, *100*, 24,487–24,498, doi:10.1029/95JB02630.

Watts, A. B., and D. G. Masson (2001), New sonar evidence for recent catastrophic collapses of the north flank of Tenerife, Canary islands, *Bull. Volcanol.*, *63*, 8–19, doi:10.1007/s004450000119.

Weaver, P. P. E. (1994), Determination of turbidity current erosional characteristics from reworked coccolith assemblages, Canary Basin, north-east Atlantic, *Sedimentology*, *41*(5), 1025–1038.

Weaver, P. P. E. (2003), Northwest Africa Continental Margin: History of sediment accumulation, landslide deposits, and hiatuses as revealed by drilling the Madeira Abyssal Plain, *Paleoceanography*, *18*(1), 1009, doi:10.1029/2002PA000758.

Weaver, P. P. E., and A. Kuijpers (1983), Climatic control of turbidite deposition on the Madeira Abyssal Plain, *Nature*, *306*, 360–363.

Weaver, P. P. E., and R. G. Rothwell (1987), Sedimentation on the Madeira Abyssal Plain over the last 300,000 yrs, in *Geology and Geochemistry of Abyssal Plains*, vol. 31, edited by P. P. E. Weaver and J. Thomson, pp. 71–86, Geol. Soc. Spec. Publ., London, U. K.

Weaver, P. P. E., and J. Thomson (1993), Calculating erosion by deep-sea turbidity currents during initiation and flow, *Nature*, *364*(6433), 136–138.

Weaver, P. P. E., R. G. Rothwell, J. Ebbing, D. Gunn, and P. M. Hunter (1992), Correlation, frequency of emplacement and source directions of megaturbidites on the Madeira Abyssal Plain, *Mar. Geol.*, *109*, 1–20.

Wynn, R. B., and D. G. Masson (2003), Canary island landslides and tsunami generation: Can we use turbidite deposits to interpret landslide processes, in *First International Symposium on Submarine Mass Movements and Their Consequences, Adv. in Nat. and Technol. Hazards Res.*, vol.19, edited by J. Locat and J. Mienert, pp. 325–332, Kluwer Acad. Publ., Dordrecht, Netherlands.

Wynn, R. B., D. G. Masson, D. A. V. Stow, and P. P. E. Weaver (2000), The Northwest African slope apron: A modern analogue for deep-water systems with complex seafloor topography, *Mar. Petrol. Geol.*, *17*(2), 253–265.

Wynn, R. B., P. P. E. Weaver, D. A. V. Stow, and D. G. Masson (2002), Turbidite depositional architecture across three interconnected deep-water basins on the northwest African margin, *Sedimentology*, *49*, 1441–1462, doi:10.1046/j.1365–3091.2002.00471.x.